1, Gary Rankin

5. CONTRACT NAS9-16399
DRL T-1663, Item 3
DRD MA-1837TH

NASA-CR-167625

2. TESTING OF A HIGH CAPACITY RESEARCH HEAT PIPE

FINAL REPORT

6. MAY 1982

7. SSD82-0092

Prepared for

Lyndon B. Johnson Space Center
National Aeronautics and Space Administration
Houston, Texas

4.

Space Operations/Integration &
Satellite Systems Division

Rockwell International

TECHNICAL REPORT INDEX/ABSTRACT

ACCESSION NUMBER						DOCUMENT SECURITY CLASSIFICATION	
						Unclassified	

TITLE OF DOCUMENT

Testing of a High Capacity Research Heat Pipe

LIBRARY USE ONLY

AUTHOR(S)
Lehtinen, Arthur M.

CODE	ORIGINATING AGENCY AND OTHER SOURCES	DOCUMENT NUMBER
QN085282	Rockwell International Corporation Space Systems Group Downey, California	SSD82-0092

PUBLICATION DATE	CONTRACT NUMBER
May 1982	NAS9-16399

DESCRIPTIVE TERMS

Heat pipe, high capacity heat pipe, capillary pumping, groove transport, boiling, heat transfer, 2-phase heat transfer

ABSTRACT

Tests were performed on Rockwell's high-capacity channel-wick heat pipe to assess the transport limitations of v-grooves and the effects of boiling. The results showed that transport can vary significantly (>50W) under similar conditions and that continuous boiling was observed at power levels as low as 40 W. In addition, some evidence was found to support the predictions using a groove transport model which shows that transport increases with lower groove densities and longer evaporators. However, due to transport variations, these results were not consistent throughout the program. When a glass fiber wick was installed over the grooves, a relatively low transport level was achieved (80-140 W). Based on these results and the identification of some potential causes for them, several design suggestions were recommended for reducing the possibility of boiling and improving groove transport.

Contract NAS9-16399
DRL T-1663, Item 3
DRD MA-1837TH

TESTING OF A HIGH CAPACITY RESEARCH HEAT PIPE

FINAL REPORT

MAY 1982 SSD82-0092

Prepared for

Lyndon B. Johnson Space Center
National Aeronautics and Space Administration
Houston, Texas

by

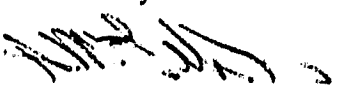

A. M. Lehtinen
Program Manager

Approved by:

J. P. Wright

J. P. Wright, Supervisor
Aerothermal Systems

L. M. Smith FOR

L. L. Bissing, Manager
S/C Mechanical & Fluid Systems

Space Operations/Integration &
Satellite Systems Division

Rockwell International

FOREWORD

This report is submitted by the Space Operations/Integration and Satellite Systems Division of Rockwell International Corporation to the National Aeronautics and Space Administration, Lyndon B. Johnson Space Center in accordance with the requirements of Contract NAS9-16399. The work was administered by the System Engineering Branch of the Crew Systems Division with Gary Rankin as Technical Monitor.

The program covered the period from June 1981 to May 1982 and was under the direction of A. M. Lehtinen, Program Manager. Technical and Laboratory assistance was provided by G. W. Gurr and H. T. Nguyen.

ABSTRACT

Tests were performed on Rockwell's high-capacity channel-wick heat pipe to assess the transport limitations of v-grooves and the effects of boiling. The results showed that transport can vary significantly (>50 W) under similar conditions and that continuous boiling was observed at power levels as low as 40 W. In addition, some evidence was found to support the predictions using a groove transport model which shows that transport increases with lower groove densities and longer evaporators. However, due to transport variations, these results were not consistent throughout the program. When a glass fiber wick was installed over the grooves, a relatively low transport level was achieved (80-140 W). Based on these results and the identification of some potential causes for them, several design suggestions were recommended for reducing the possibility of boiling and improving groove transport.

CONTENTS

ILLUSTRATIONS

TABLES

NOMENCLATURE

A - Area
f·Re - Friction coefficient
L - Length
N_g - Groove density
N_ℓ - Liquid transport factor
P - Pressure, perimeter
$\dot{Q}$ - Heat transport
T - Temperature
V - Velocity
d/d_i - Groove depth quality
g - Standard gravity
h - Tilt, film coefficient
k - Liquid thermal conductivity
$\dot{m}$ - Mass flow
r - Radius, pumping radius
s - Slab width
w - Channel width
w/p - Groove pitch quality
Δ - Difference operator
α - Contact angle
β - Constant
γ - $\pi/2 - \alpha - \phi$
δ - Channel depth
λ - Heat of vaporization
μ - Dynamic viscosity
υ - Kinematic viscosity
ρ - Density
σ - Surface tension
ϕ - Groove half-angle

Subscripts
b - Body forces
c - Capillary
e - Evaporator
eff - Effective
n - Nucleation
p - Pore
sh - Superheat
v - Vapor
w - Wetted
ℓ - Liquid

1.0 INTRODUCTION

A number of future space based systems will need high capacity heat pipes to meet the requirements of long life and system reliability. Some of the currently proposed applications for high capacity heat pipes are in the areas of large space constructable radiators, space stations, large space platforms,and space processing ovens.

In meeting these future requirements there are two primary problems. They are(1) the system's sensitivity to micrometeoroid damage and (2) component reliability. In the case of a penetration by a micrometeoroid, a fluid loop or a heat pipe will be disabled. However, in the heat pipe system, only one pipe in the system will be lost, thus minimizing the effects on the overall system performance. On the other hand the loss of a single tube in a typical fluid loop system could disable a substantial portion of the thermal control system.

The other potential problem is that the fluid loop contains active components (such as pumps, valves, refrigerators, etc.) which have a relatively limited lifetime. As a result, the components will require periodic replacement, maintenance, or a complex backup system to attain the desired overall system reliability.

Consequently, from life cycle considerations, a passive heat pipe thermal control system appears to be desirable for systems with lifetimes greater than five years. One of the critical components in this design approach is the development of a high capacity heat pipe. The near term needs will require transport capacities of 10-20 kW-m. Future requirements will probably exceed the 100 kW-m capability. In addition to these requirements, the evaporator interface area will need to be minimized to facilitate space assembly and radiator effectiveness.

It is this latter problem that this program addresses. In particular, this program was aimed at testing the overall pipe performance as a function of various evaporator design parameters. The primary objective of this testing was to obtain test data that would aid in developing future design approaches

for high capacity heat pipes. The program scope was limited to testing Rockwell's channel wick concept using ammonia as the working fluid. The results of these tests were then correlated to try and identify some general characteristics of the various evaporators tested.

2. HEAT PIPE DESCRIPTION

Figure 2-1 shows the basic channel-wick heat pipe concept. Basically, it consists of 2 axial channels which run the length of the pipe and act as the main liquid transport passages for the working fluid. In addition, v-grooves have been cut on the evaporating and condensing surfaces as shown in Figure 2-1. These grooves act to distribute the liquid over the heating surface and provide the primary pumping for the pipe. On the fill tube end of the pipe, the groove density is 20 grooves/cm (50 grooves/inch), while on the opposite end the groove density is 39 grooves/cm (100 grooves/inch).

Two isolator slots were cut into heating interface slab and filled with fiberglass epoxy. These slots help retard the heat flow into the channels, thus reducing the boiling potential.

This basic configuration was modified in 1980 to the one shown in Figure 2-2. The cover blocks were added to help correct flaws in the grooved surfaces. An aluminum foil gasket was also added to help conform to the groove tips. These modifications increased the pipe bubble pressure from 1.8 to 2.5 cm H_2O (.7 to 1.0 in. H_2O).

In addition, polysulfone windows were added to each end of the pipe for observation of the evaporator and condenser sections. These windows were bonded to the aluminum surface using RTV-566, which is a low outgassing adhesive. The adhesive was used to seal the windows as well as help minimize window deflections which could cause the RTV bond to tear and leak. Backer plates and cross members were also used to minimize this deflection of the window.

Another modified configuration was tested during the program as shown in Figure 2-3. This configuration is similar to the first modification except that glass fiber wick was installed underneath the cover blocks. The intent of this modification was to improve the liquid distribution over the grooves.

A picture of the hardware is shown in Figure 2-4. In addition, Figure 2-5 shows a close-up of the window assembly.

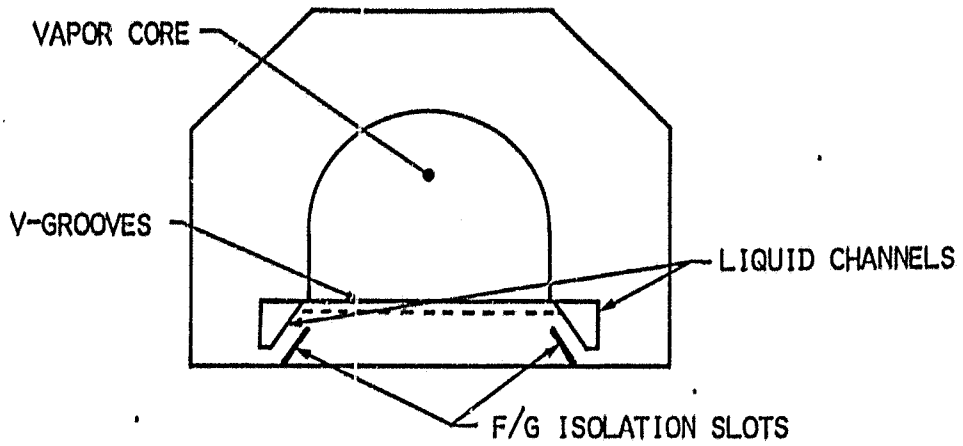

Figure 2-1. Basic Channel-Wick Heat Pipe Concept.

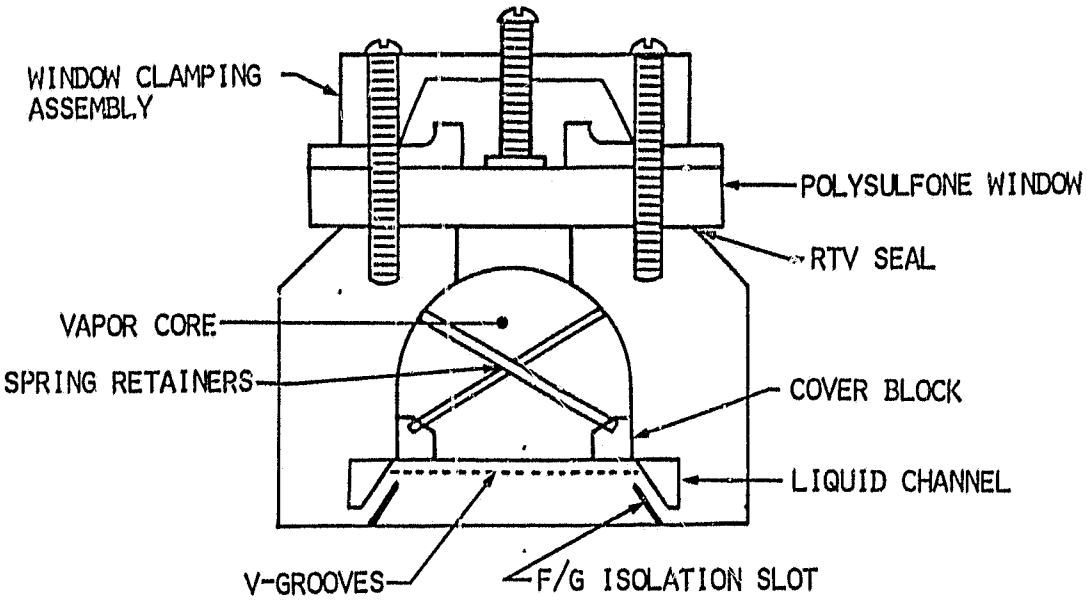

Figure 2-2. Modified Channel-Wick Heat Pipe Concept.

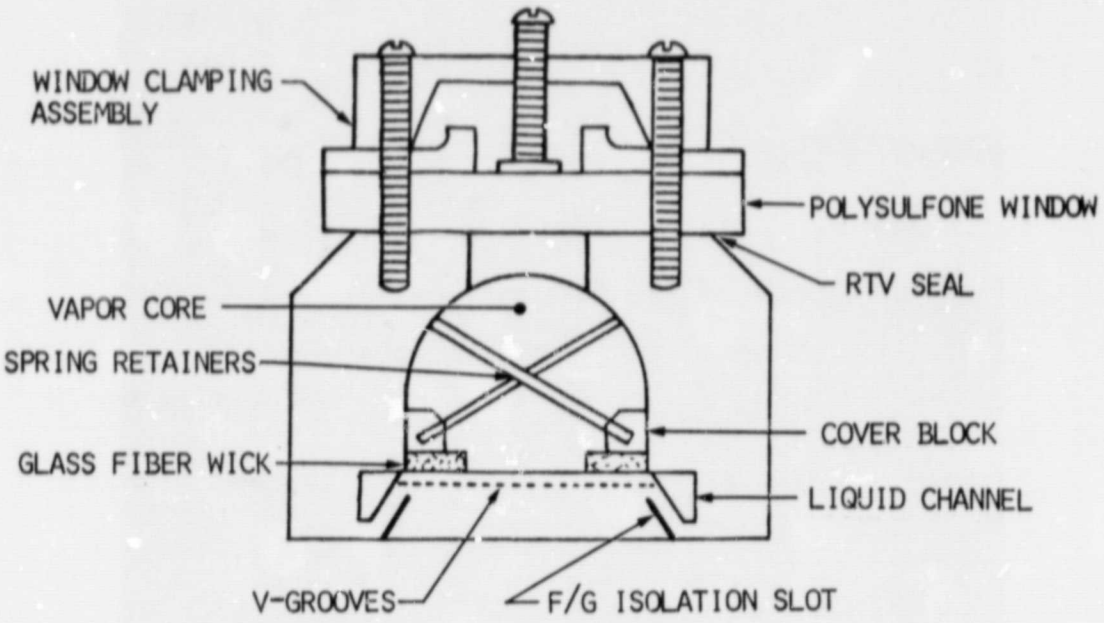

Figure 2-3. Glass-Fiber Wick Modification.

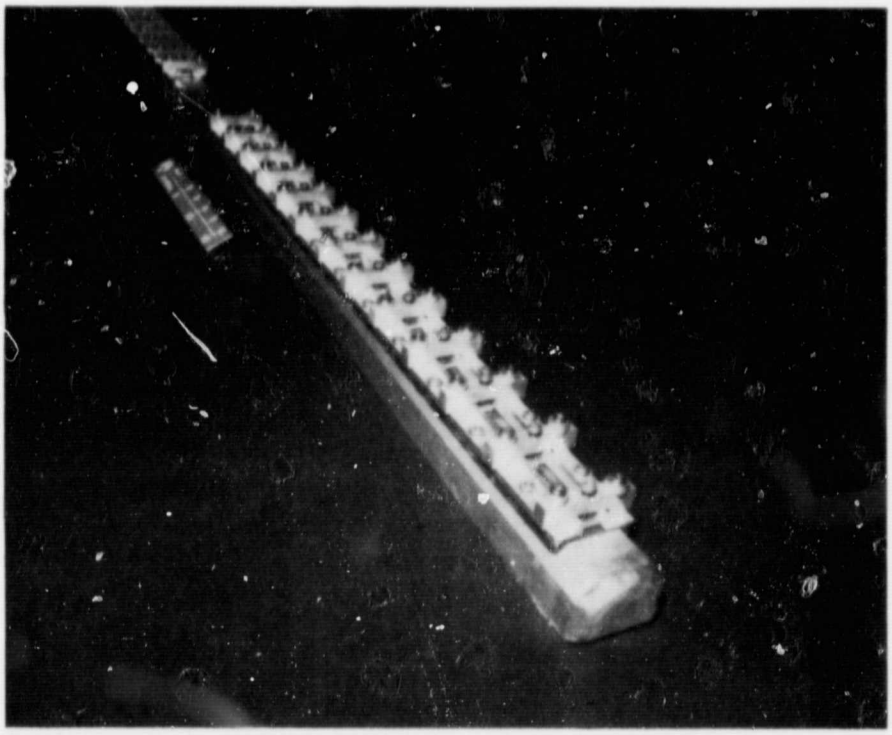

Figure 2-4. Modified Channel-Wick Hardware.

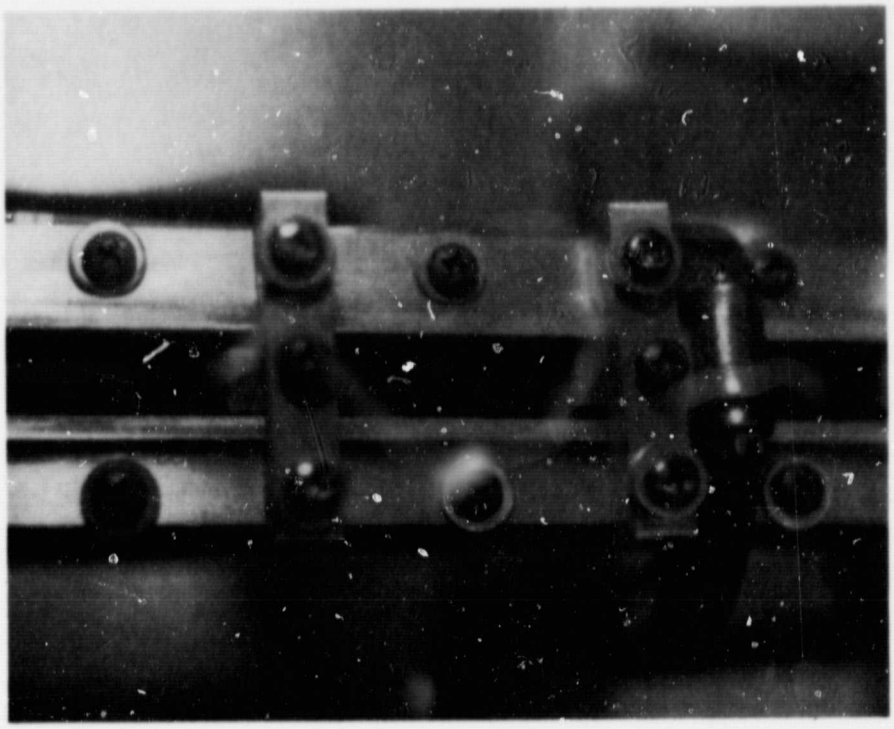

Figure 2-5. Heat Pipe Window Assembly Close-Up.

3. PRE-TEST ANALYSIS

Several factors can limit the maximum capability of the channel-wick heat pipe. These include the channel transport, the groove transport, boiling, and non-condensible gas contamination. The channel transport limit (also generally known as the capillary limit) results from the inability of the capillary pressure to supply enough liquid to the evaporator for steady state operation. Generally, this limit is the basis for developing high capacity heat pipe designs. Figure 3-1 shows this limit and the design problem of matching this limit with the groove transport limit, which will be discussed next.

The groove transport limit results when the grooves cannot maintain an adequate supply of liquid over the v-groove surface. Theoretically, this is analyzed as a capillary pumping process. However, due to some real and theoretical considerations, this analysis is only an approximation. However, under relatively low heat fluxes this approximation should be relatively accurate. On the other hand, under high heat fluxes, boiling is likely to occur and the results would be expected to differ significantly. The boiling process results from spontaneous bubble growth at nucleation sites on the evaporating surface. The point at which this process becomes destructive and limits heat pipe performance is not yet fully understood. However, it is believed that various evaporator design characteristics and gas do contribute to this limit. Because boiling is not well understood, testing is the only method of estimating the boiling limit.

The final problem that limits heat pipe performance is the presence of non-condensible gas. Basically, this limit occurs when a relatively small amount of gas is trapped in the liquid channel. This acts to destroy the capillary pumping capability and thus causes channel transport failure.

As can be seen, all of these transport failure mechanisms are interrelated. For example, the channel transport limit, the groove transport limit, and gas contamination all affect the capillary pumping capability of the pipe. On the other hand, the groove transport limit, the boiling limit,

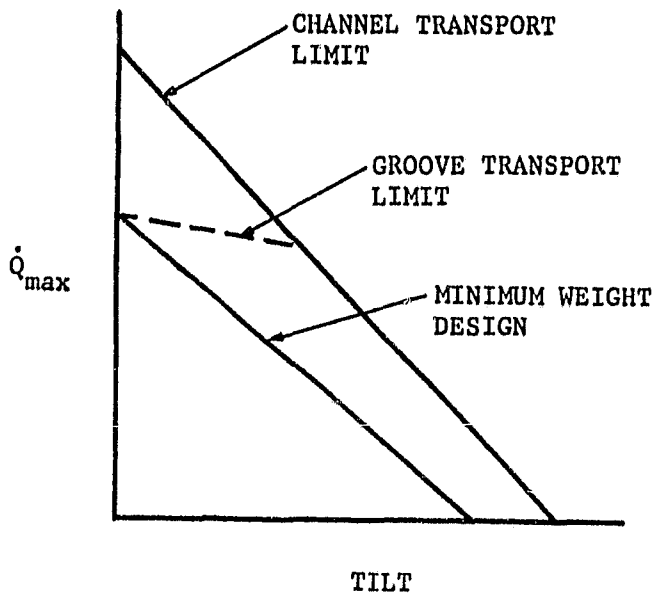

Figure 3-1 Channel/Groove Transport Design Problem

and gas contamination are related since boiling is probably the mechanism that causes transport failure and gas will probably contribute to the sensitivity of the boiling process.

CHANNEL TRANSPORT ANALYSIS

The system pressure balance for the channel-wick heat pipe is described by the following equation:

$$P_c = \Delta P_\ell + \Delta P_v + \Delta P_b \tag{3-1}$$

where

$$P_c = \frac{\sigma}{r} \tag{3-2}$$

$$\Delta P_\ell = \frac{\mu_\ell P_{w\ell}^2}{32\lambda\rho_\ell A_\ell^3} (f\cdot Re)_\ell (\dot{Q}\cdot L_{eff}) \tag{3-3}$$

$$\Delta P_v = \frac{\mu_v P_{wv}^2}{32\lambda\rho_v A_v^3} (f\cdot Re)_v (\dot{Q}\cdot L_{eff}) \tag{3-4}$$

and

$$\Delta P_b = (\rho_\ell - \rho_v)gh \tag{3-5}$$

Substituting Equations 3-2 through 3-5 into Equation 3-1 and rearranging yields the following transport equation:

$$\dot{Q}\cdot L_{eff} = \frac{32N_\ell(1/r - (\rho_\ell - \rho_v)gh/\sigma)(A_\ell^3/P_{w\ell}^2)}{((f\cdot Re)_\ell + (\nu_v/\nu_\ell)(A_\ell/A_v)^3(P_{wv}/P_{w\ell})^2(f\cdot Re)_v)} \tag{3-6}$$

where

$$N_\ell = \frac{\sigma \rho_\ell \lambda}{\mu_\ell}$$

For channels with aspect ratios (δ/w) greater than 1.5, the following equation yields a reasonable approximation of the liquid friction coefficient $(f \cdot Re)_\ell$ (Reference 1).

$$(f \cdot Re)_\ell = \frac{96}{(1 + w/\delta)^2 (1 - .627(w/\delta))} \qquad (3\text{-}7)$$

The vapor friction coefficient $(f \cdot Re)_v$ is given by one of the following equations:

$$(f \cdot Re)_v = 64 \qquad \text{for} \quad Re \leqslant 2100 \qquad (3\text{-}8)$$

or

$$(f \cdot Re)_v = .316(Re_v)^{.75} = .316\left[\frac{4\dot{Q}}{\mu_v \lambda P_{wv}}\right]^{.75} \qquad \text{for} \quad Re \geqslant 2100 \qquad (3\text{-}9)$$

Equations 3-6 through 3-9 have been integrated into a computer program which solves for the transport as a function heat pipe tilt.

The results for the current channel-wick heat pipe are shown in Figure 3-2. As can be seen, the maximum transport is 15.5 kW for the 39 groove/cm (100 groove/inch) evaporator and 8.1 kW for the 20 groove/cm (50 groove/inch) evaporator. Also, the static heights are 1.2 cm and 2.5 cm for the 20 and 39 groove/cm evaporators, respectively.

GROOVE TRANSPORT ANALYSIS

The primary problem in reaching the channel transport limit is that the evaporator grooves burnout and this induces premature pipe failure. The groove burnout results from relatively high heat fluxes to the evaporator section. Consequently, long evaporators with low heat fluxes will tend to approach the channel transport limit. However, this design approach is un-

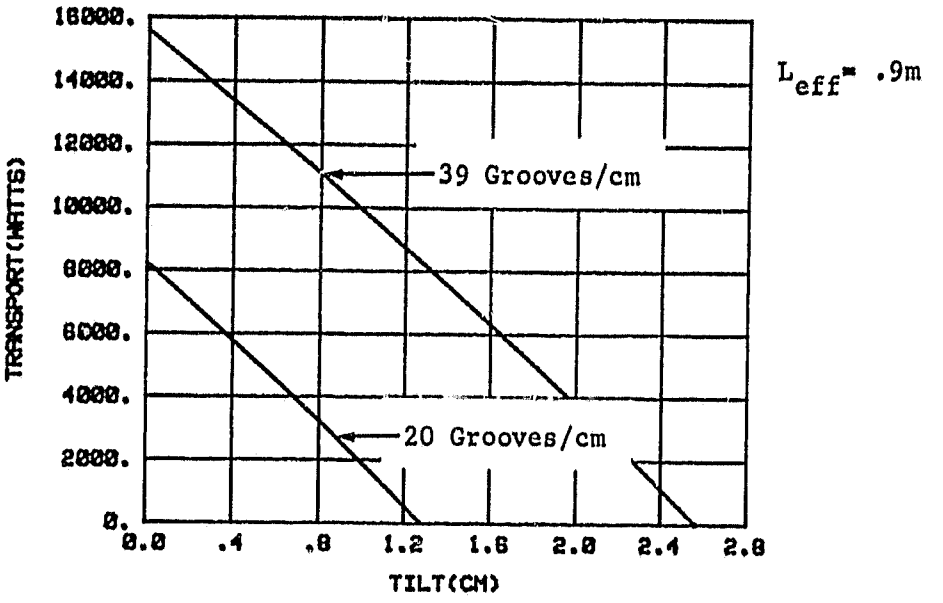

Figure 3-2. Channel Wick Transport

desirable from a systems standpoint since it is difficult to integrate and increases the thermal control system weight.

An analysis was developed in Reference 2 which evaluates how the evaporator length can be minimized. The basic approach to this analysis will be summarized here along with the results relative to the current channel wick heat pipe design. This will be followed by a short discussion of the results and a summary of what the tests were expected to yield.

Groove Transport Model

Figure 3-3 shows the basic model for developing the groove transport equations. This model assumes a uniform heat input along the groove and burnout is defined as the heat load at which the pumping radius reaches its minimum value. It is also assumed that the transport of the channels has been matched to the grooved evaporator (See Figure 3-1). Matching is desirable since it helps minimize the channel wick weight. The effect of this latter assumption is that the entry pore radius is tangent to the groove tips.

Along the groove, the capillary pressure is defined as

$$P_c = \frac{\sigma}{r}$$

Differentiating and rearranging this equation gives the equation for capillary pumping across an element dx.

$$dP_c = -\frac{\sigma}{r^2}\, dr \qquad (3\text{-}10)$$

The pressure loss across the element dx is given by

$$dP_\ell = -\frac{f \rho_\ell V_\ell^2}{2 D_\ell} dx = -\frac{\mu_\ell (f \cdot Re)_\ell V_\ell}{2 D_\ell^2} dx$$

Since the v-grooves in the channel wick are flat, the gravity effects can be ignored and the pressure balance equation becomes

$$dP_c = -dP_\ell$$

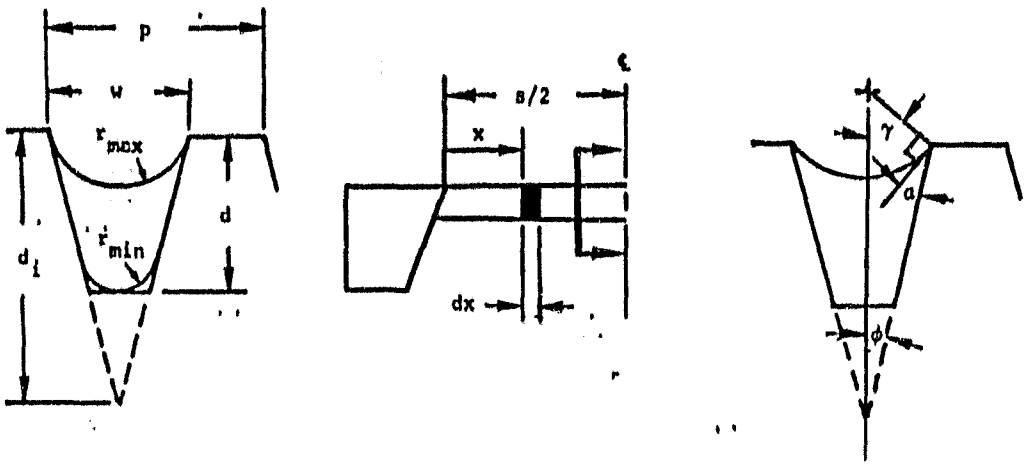

Figure 3-3. Grove Transport Model

or

$$\frac{\sigma}{r^2}\,dr = -\frac{\mu_\ell\,(f\cdot Re)_\ell\,V_\ell\,P_w^2}{32A_\ell^2}\,dx \qquad (3\text{-}11)$$

The liquid velocity (V_ℓ) can be derived from the continuity equation and the assumption of uniform heat flux along the groove. As a result of the uniform heat flux assumption, the liquid mass flow decreases uniformly as follows:

$$\frac{d\dot{m}}{dx} = -\frac{\dot{Q}}{\lambda N_g L_e s}$$

Consequently, at any point "x" (where $0 \le x \le s/2$) along the groove the liquid influx is

$$\dot{m}_x = \frac{\dot{Q}}{2\lambda N_g L_e}\left[1 - \frac{2x}{s}\right]$$

Therefore, the velocity at point "x" is

$$V_\ell = \frac{\dot{Q}}{2\lambda \rho_\ell A_\ell N_g L_e}\left[1 - \frac{2x}{s}\right] \qquad (3\text{-}12)$$

Substituting this into Equation 3-11 and rearranging yields the following differential equation:

$$-\frac{64\,N_\ell\,N_g\,L_e}{(f\cdot Re)_\ell}\,\frac{A_\ell^3}{P_w^2}\,\frac{dr}{r^2} = \dot{Q}\left[1 - \frac{2x}{s}\right]dx \qquad (3\text{-}13)$$

Using the geometry in Figure 3-3, the following equation can be derived for the liquid area as a function of "r":

$$A_\ell = r^2\left[\frac{\cos(\alpha)\,\sin(\gamma)}{\sin(\phi)} - \gamma\right] - \frac{(w/p)^2(1 - d/d_i)^2}{4N_g^2\tan(\phi)} \qquad (3\text{-}14)$$

where w/p and d/d_i are the groove pitch and depth qualities, respectively. Also, assume that the wetted perimeter can be approximated by

$$P_W = 2r \frac{Sin(\gamma)}{Sin(\phi)} \tag{3-15}$$

For poorer depth qualities (small values of d/d_i), this assumption will likely result in significant errors. In addition, the liquid friction coefficient $(f \cdot Re)_\ell$ is assumed equal to its ideal value ($d/d_i = 1$) and thus contributes to this error. As a consequence of these errors the predicted transport values are expected to be lower than what more detailed calculations would yield. Therefore, these predictions should be conservative and useful for preliminary design analyses.

Substituting Equations 3-14 and 3-15 into Equation 3-13 and integrating between r_{max} and r_{min}, where

$$r_{max} = \frac{(w/p)}{2 N_g Sin(\gamma)} \qquad @ \quad x = 0$$

and

$$r_{min} = \frac{(w/p)(1 - d/d_i)}{2 N_g (Sin(\gamma) + Tan(\phi)(Cos(\gamma) - 1))} \qquad @ \quad x = \frac{s}{2}$$

gives the following groove transport equation:

$$\dot{Q} = \frac{8 N_f L_e (w/p)^3 Sin^2(\phi)}{(f \cdot Re) N_g^2 s \, Sin^2(\gamma)} \left[w_1 - w_2 - w_3 + w_4 \right] \tag{3-16}$$

where

$$w_1 = \frac{D_1^3}{3} \left[A_2^3 - A_1^3 \right]$$

$$w_2 = \frac{3 D_1^2 (1 - d/d_i)^2}{Tan(\phi)} \left[A_2 - A_1 \right]$$

$$W_3 = \frac{3D_1(1 - d/d_i)^4}{\mathrm{Tan}^2(\phi)} \left[A_2^{-1} - A_1^{-1}\right]$$

$$W_4 = \frac{(1 - d/d_i)^6}{3\mathrm{Tan}^3(\phi)} \left[A_2^{-3} - A_1^{-3}\right]$$

$$D_1 = \frac{\mathrm{Cos}(\alpha)\ \mathrm{Sin}(\gamma)}{\mathrm{Sin}(\phi)} - \gamma$$

$$A_1 = \frac{(1 - d/d_i)}{(\mathrm{Sin}(\gamma) + \mathrm{Tan}(\phi)(\mathrm{Cos}(\gamma) - 1))}$$

$$A_2 = \frac{1}{\mathrm{Sin}(\gamma)}$$

Analytical Results

From Equation 3-16, it can be seen that the transport varies directly with the evaporator length, inversely with the grooved slab width, and with the inverse square of the groove density. In addition, the bracketed term in Equation 3-16 defines how groove quality degrades pipe performance.

Figures 3-4 and 3-5 define the transport characteristics for the 30 and 61 cm evaporators with a 2.54 cm slab width. Similarly, Figures 3-6 and 3-7 show the results for a 1.27 cm slab width. The upper curve in each figure defines the transport characteristics for an ideal groove ($w/p = 1$, $d/d_i = 1$), while the two lower curves bracket the expected real transport range.

As can be seen from these curves the groove transport tends to decrease as the groove density increases. Also, as the groove quality decreases, the predicted performance decreases significantly along with the transport sensitivity to groove density.

For real grooves, the groove quality would be expected to decrease with increasing groove density. Consequently, the real groove transport differences between two groove densities would be expected to be larger than shown. Due to the sensitivity of some of the groove parameters, the groove transport cannot be predicted accurately. Consequently, the primary objective of the test program was to establish whether these general trends exist.

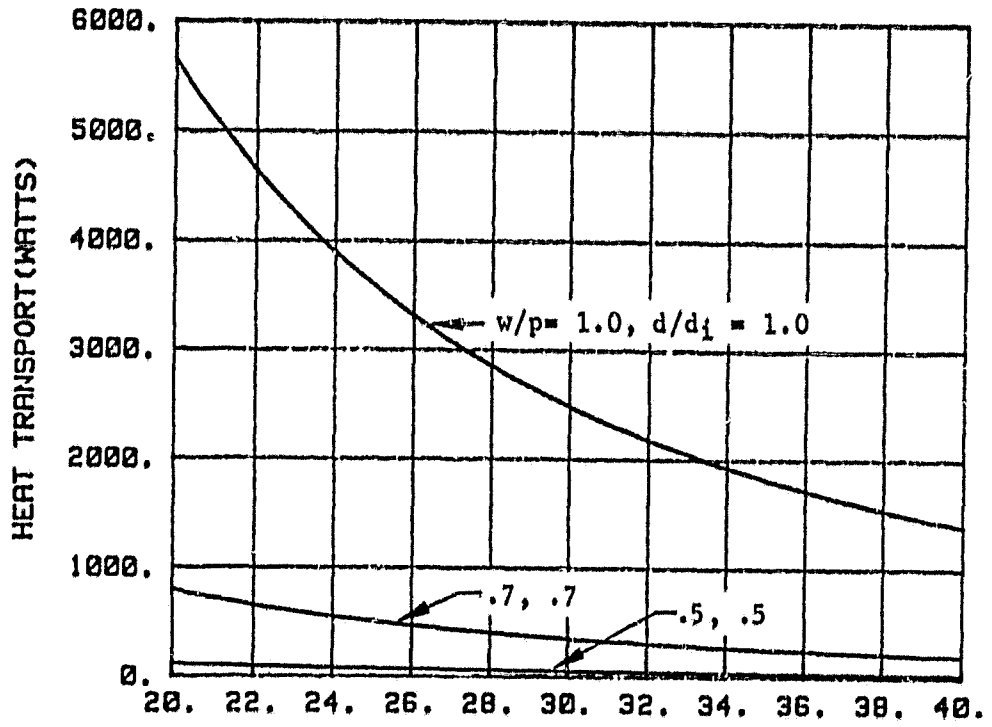

Figure 3-4. Groove Transport for the 30 cm Long, 2.54 cm Wide Evaporator.

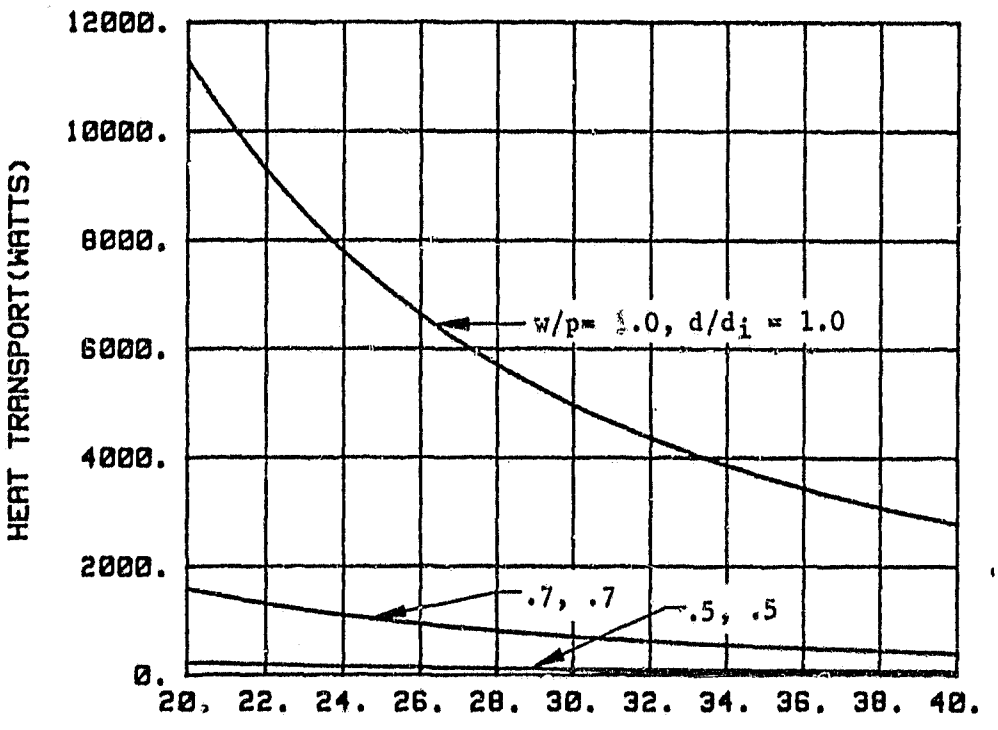

Figure 3-5. Groove Transport for the 61 cm Long, 2.54 cm Wide Evaporator.

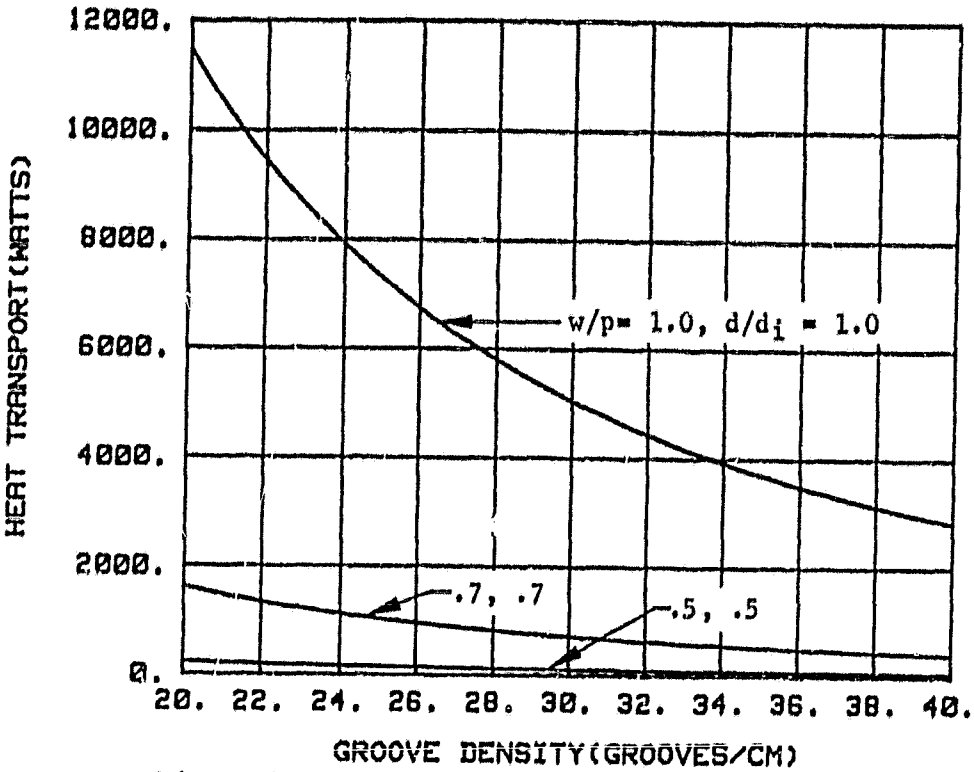

Figure 3-6. Groove Transport for the 30 cm Long, 1.27 cm Wide Evaporator.

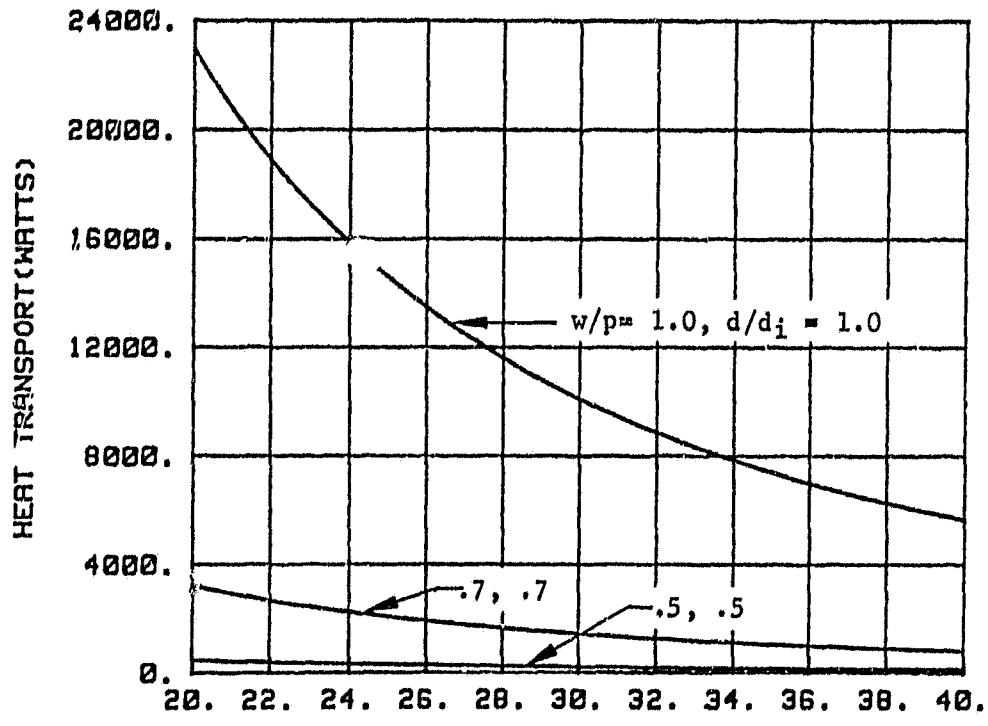

Figure 3-7. Groove Transport for the 61 cm Long, 1.27 cm Wide Evaporator.

BOILING ANALYSIS

A simplified boiling model was developed using the basic geometry shown in Figure 3-8. This model assumes that nucleation occurs when the wall superheat exceeds the temperature required to cause bubble expansion. This occurs when the following conditions are met:

$$P_n > P_\ell + \frac{2\sigma}{r_n} = P_v - P_c + \frac{2\sigma}{r_n} \qquad (3\text{-}17)$$

where $P_c = \sigma/r_p$ for the grooves.

The wall temperature required for this condition can be approximated by using the Clausius-Clapeyron equation,

$$\frac{dP}{dT} = \frac{\lambda \rho_v \rho_\ell}{T_v(\rho_\ell - \rho_v)}$$

$$dT = \frac{T_v(\rho_\ell - \rho_v)}{\lambda \rho_v \rho_\ell} dP$$

or

$$\Delta T_{sh} = \frac{T_v(\rho_\ell - \rho_v)}{\lambda \rho_v \rho_\ell} \Delta P \qquad (3\text{-}18)$$

The nucleation pore pressure (P_n) is related to the vapor pressure as follows:

$$P_n = P_v + \Delta P_v$$

Substituting this into Equation 3-17 yields the following:

$$\Delta P_v = \frac{2\sigma}{r_n} - P_c$$

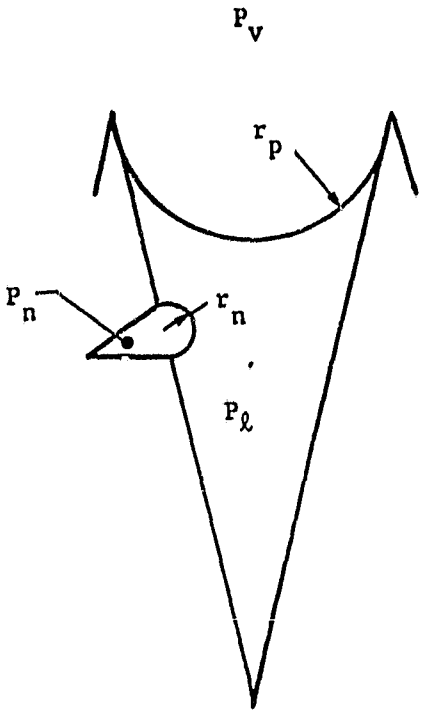

Figure 3-8. Simple Boiling Model Geometry.

Substituting this into Equation 3-18 yields

$$\Delta T_{sh} = \frac{T_v(\rho_\ell - \rho_v)}{\lambda \rho_v \rho_\ell}\left[\frac{2\sigma}{r_n} - P_c\right] \tag{3-19}$$

The general equation for the evaporator heat flux is

$$\frac{\dot{Q}}{A_e} = h_e \Delta T_e \tag{3-20}$$

where A_e is the evaporator area.

Since ΔT_e equals ΔT_{sh}, Equation 3-19 can be substituted into Equation 3-20 as follows:

$$\frac{\dot{Q}}{A_e} = \frac{h_e\, T_v\, (\rho_\ell - \rho_v)}{\lambda \rho_v \rho_\ell}\left[\frac{2\sigma}{r_n} - P_c\right]$$

Rearranging this equation gives the heat transport as:

$$\dot{Q} = \frac{h_e\, s\, L_e\, T_v\, (\rho - \rho_v)}{\lambda \rho_v\, \rho_\ell}\left[\frac{2\sigma}{r_n} - P_c\right] \tag{3-21}$$

Since the film coefficient (h_e) is expected to vary directly with the groove density (N_g) and the liquid thermal conductivity (k_ℓ), the following simplified equation is assumed for the film coefficient:

$$h_e = \beta N_g k_\ell$$

Substituting this into Equation 3-21 yields

$$\dot{Q} = \frac{\beta N_g\, k_\ell\, s\, L_e\, T_v\, (\rho_\ell - \rho_v)}{\lambda \rho_v \rho_\ell}\left[\frac{2\sigma}{r_n} - P_c\right]$$

This equation can be rearranged as follows:

$$\dot{Q} = \beta (N_g \; s \; L_e) \left[\frac{\sigma \, k_\ell \, T_v \, (\rho_\ell - \rho_v)}{\lambda \rho_v \rho_\ell} \right] \left[\frac{2}{r_n} - \frac{1}{r_p} \right]$$

As can be seen boiling varies directly with three pipe design parameters: namely the groove density (N_g), the evaporator width (s), and the evaporator length (L_e). This grouping ($N_g s L_e$) will be an important factor in trying to correlate the heat pipe test data.

The next group basically defines the boiling tolerance of the working fluid. Table 3-1 list the values of some common working fluids and gives the relative boiling tolerance using ammonia as a reference.

Table 3-1. Working Fluid Boiling Tolerance

Working Fluid	Boiling Tolerance @300 K (Watts)	Relative Boiling Tolerance @300 K *
Ammonia	30.1 E-8	1.00
Freon	28.9 E-8	.96
Acetone	256.3 E-8	8.51
Freon-11	43.8 E-8	1.45

*Ammonia is reference fluid.

Table 3-1 shows Freon-11 to be slightly more boiling tolerant than ammonia. Furthermore, acetone is shown to be significantly more tolerant than either ammonia or Freon-11. It should be emphasized that these tolerances are based on a simple superheat model which does not account for gas absorption or desorption. Consequently, small differences may not yield improved results. Therefore, out of the four fluids shown in Table 3-1, acetone has the highest probability of successfully improving the boiling tolerance.

4. HEAT PIPE PROCESSING AND SET-UP

This section presents the basic heat pipe processing procedures along with the heat pipe test set-up. The processing procedures outline the proof pressure and leak tests, the bakeout procedures, and the fill procedures. The test set-up and instrumentation used for acquiring the test data are also described.

PROOF PRESSURE AND LEAK TESTS

After each time the windows were replaced, a proof pressure test and a leak test were performed to check the pipe integrity. For the proof pressure test, the pipe was pressurized to 300 psig with GN_2 for 10 minutes. This test was followed by a helium leak check. In this test, the pipe was placed under vacuum and a helium source placed near the window seals. This test checked for leaks down to 10^{-5} STD-cc/sec.

BAKE-OUT AND FILL

The pipe was baked out for a minimum of eight hours under a vacuum of less than 10 microns. In addition, a LN_2 liquid trap in the vacuum system condensed the outgassing products. During this period, the pipe temperature was maintained at about 40° C (100° F) to enhance the outgassing process. The 40° C bake-out temperature was selected as a compromise between the desire to bake-out at a higher temperature (100-120° C) and the concern over possible damage to the RTV adhesive seal and the window optical quality. This bake-out process was repeated each time the pipe was refilled.

After the glass fiber wick was installed and prior to the installation of the windows, the pipe was vacuum baked in the 16 inch diameter vacuum chamber in the Thermal Vacuum Laboratory. During this bake-out process the pipe was maintained at about 100° C and a pressure of less than 10^{-5} microns for eight hours.

The fill procedure for this heat pipe was basically a condensation fill. Again, the polysulfone windows required a deviation from the normal Rockwell filling procedures of using LN_2 (77 K) to provide the condensation sink temperature. As an alternative, an ice bath was used for the sink temperature.

Figure 4-1 shows the basic fill set-up. This system consists of an ammonia bottle, a vacuum tee, a control volume, a vacuum system with a LN_2 liquid trap, a feed tube and the associated valving for control.

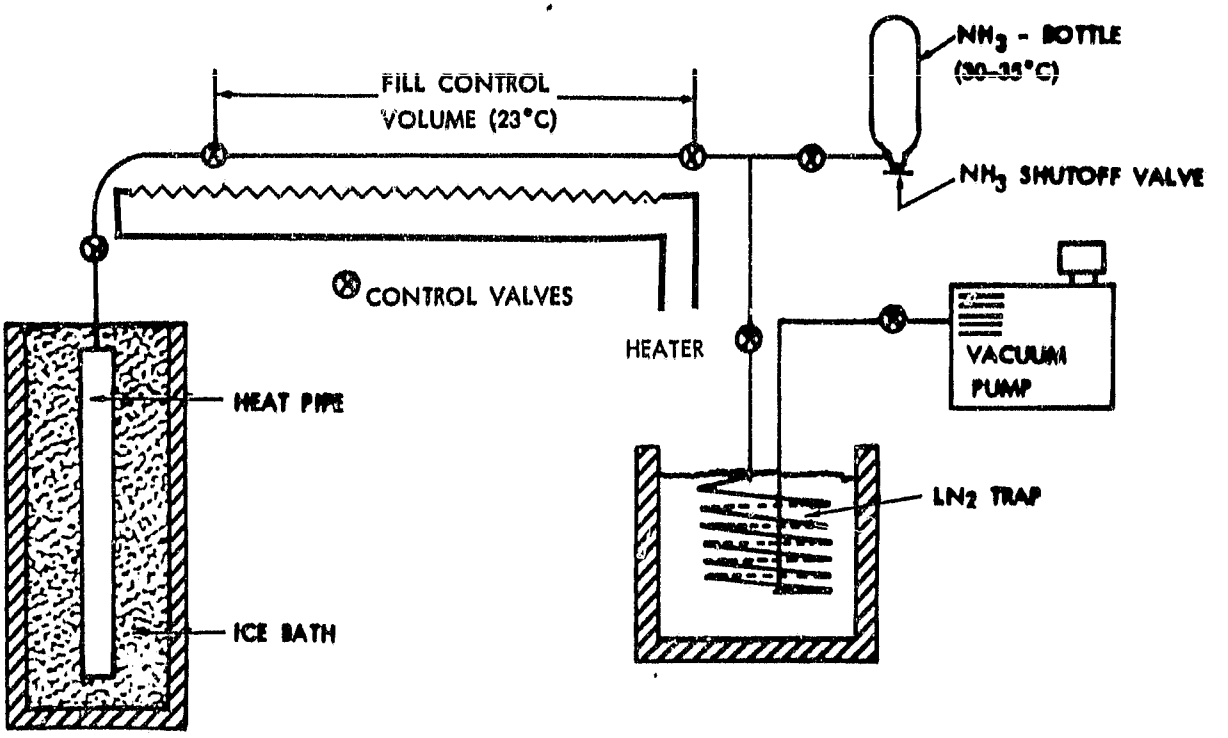

Figure 4-1 Modified Fill Set-Up

Basically, the fill procedure requires the following five steps:

1. Fabricate a control volume based on the specific fill requirements and install it in the fill fixture.
2. Place heat pipe in ice bath and allow it to cool.
3. Evacuate the pipe and fill system up to the ammonia bottle valve.
4. Fill the control volume with liquid ammonia and allow it to stabilize prior to valving off the control volume inlet.
5. Open the valves to the pipe and heat the control volume and feed tube to maximize charge transfer.

Research grade 5 ammonia (99.999% NH_3) was used for all fills during this test program to minimize the possibility of introducing gas into the heat pipe. The particular charges used for each test sequence are discussed in Section 5.

This basic fill procedure was modified somewhat for the last test sequence which involved testing the pipe with the glass fiber wick. In this case, the fill requirement could not be accurately estimated due to the uncertainty over the liquid retention in glass fiber. Therefore, a reservoir filled with ammonia was attached to the heat pipe as shown in Figure 4-2 and used to add ammonia as required. To insure an adequate fill, the evaporator v-grooves were observed through the window and ammonia was added until the grooved surface was well wetted. Also, since the reservoir was filled separately from the pipe, the normal filling procedures could be used. This allowed the use of a LN_2 bath to freeze the ammonia into the reservoir as shown in Figure 4-3. In addition, the frozen ammonia was exposed to vacuum for a minimum of 3 minutes to further minimize gas in the pipe.

TEST SET-UP

The test set-up consists of the 5 foot channel-wick heat pipe mounted on a sink bench with leveling blocks (Figure 4-4). The condenser is cooled by a water spray bar which provides 10° C water at 40-60 psig. On the evaporator end of the pipe, two 30 cm (12 in.) heater blocks are attached end-to-end. They were variac-controlled to apply a variable heat flux. The end heater

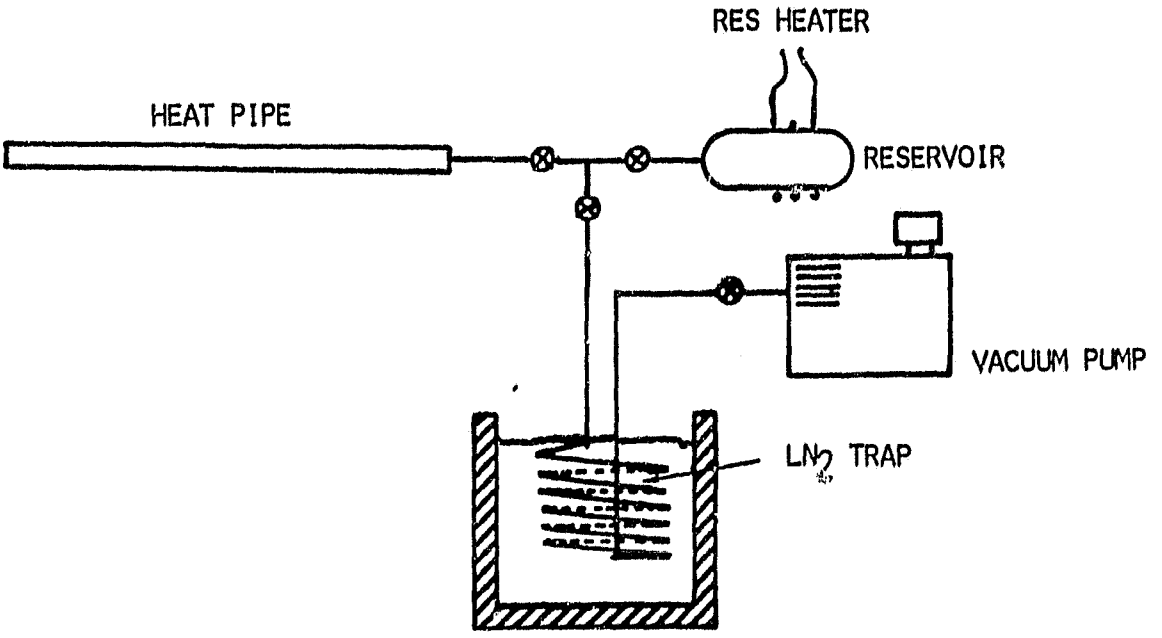

Figure 4-2. Fill Set-Up for Pipe with Glass-Fiber Wick.

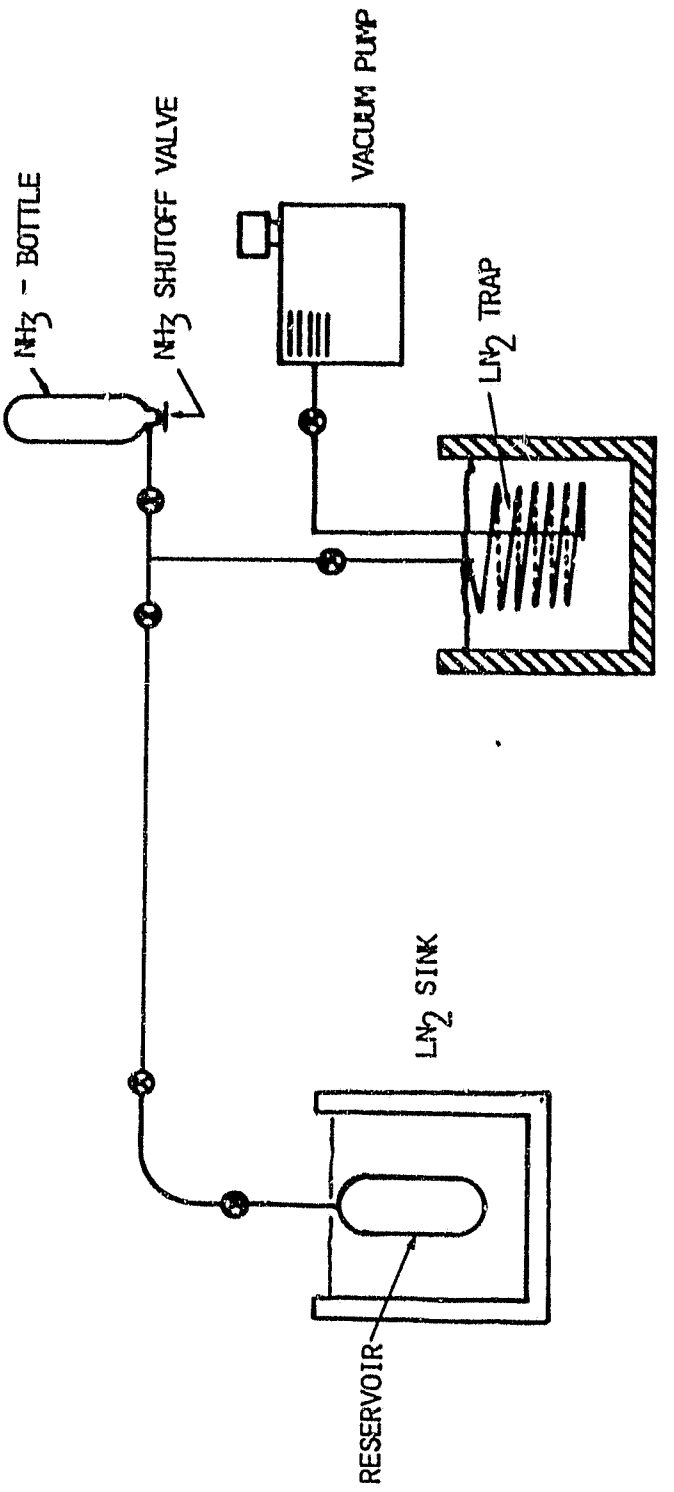

Figure 4-3. Reservoir Fill Set-Up.

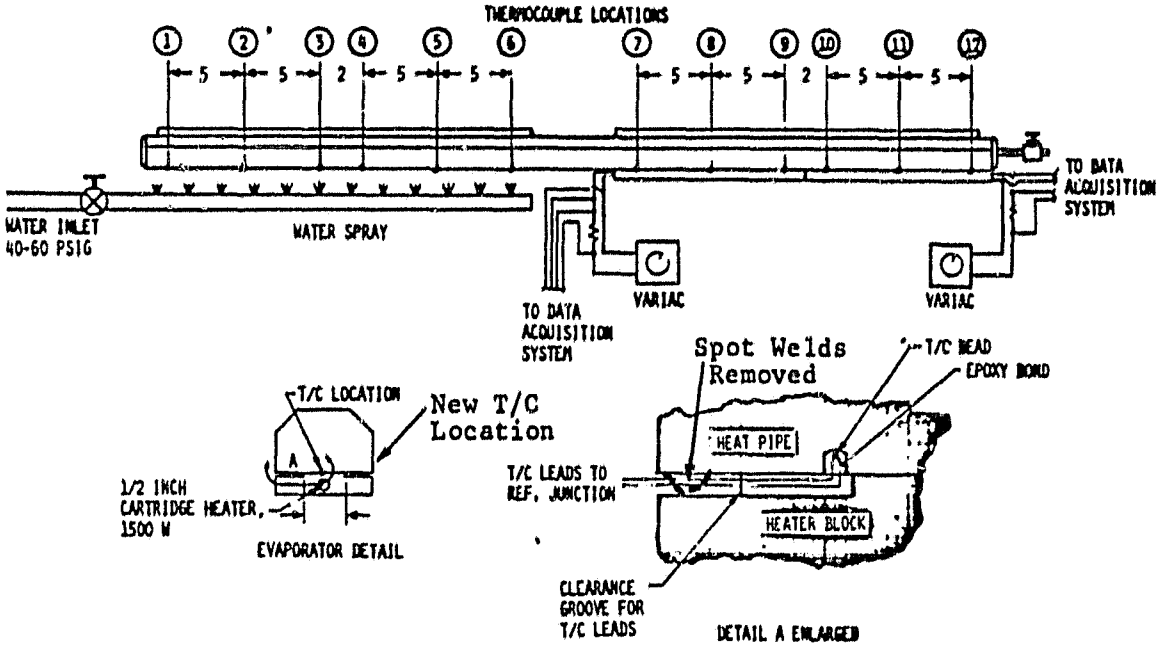

Figure 4-4. Heat Pipe Test Set-Up.

block contains two 1500 watt Cal-rod heaters; these provide a maximum evaporator heat flux of 39 W/cm^2 (based on the 2.54 cm wide heater interface). The inner heater block contained a single 1500 watt Cal-rod heater. This heater is used in conjunction with one of the heaters in the end block to provide a 19W/cm^2 heat flux capability. The evaporator groove density can be changed by simply reversing the pipe in this test set-up. The groove density was 20 grooves/cm (50 grooves/in.) at one end of the pipe and 39 grooves/cm (100 grooves/inch) at the other end.

An alternate test set-up was also used during the program in an attemp to improve the heat pipe performance. In this test set-up the pipe was canted about 20° and the heater block was moved to one edge of the evaporator as shown in Figure 4-5. This test relies on the lower liquid channels to provide the primary pipe pumping. It moves the heat application zone away from this channel and reduces the possibility of channel boiling. Also, the heat application zone is moved away from the lower cover block; this minimizes the possibility of nucleation under this block. Nucleation under the cover block is a potential cause of the meniscus recessing back into the channel area.

To reduce the transport of the channel directly above the heater block, the pipe charge was underfilled about 15% and the pipe was canted 10-20° as shown in Figure 4-5. This canting of the pipe also insured 1-G priming of the operating channel.

The polysulfone windows on the pipe provided a means for observing the evaporator and condenser sections for signs of boiling and dryout. During the tests, the optical quality of these windows slowly degraded, thus obscuring the view of the grooved surfaces. Further details of this degradation process are included in the Appendix.

INSTRUMENTATION

Two sets of thermocouples were attached to the heat pipe as shown in Figure 4-4. One set was placed underneath the pipe on the heating and cooling interfaces. The thermocouple beads were placed inside small wells

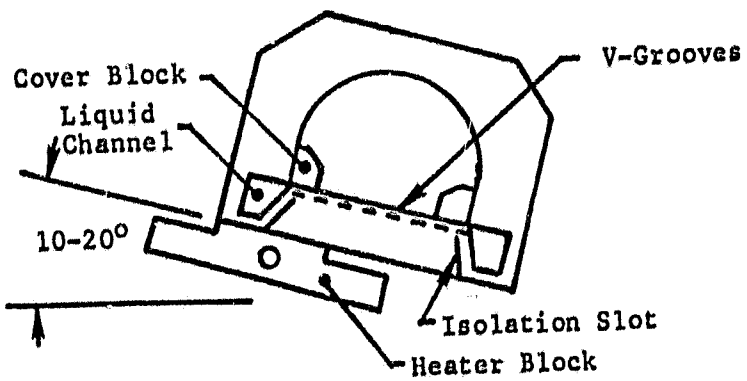

Figure 4-5. Alternate Heater Block Test Set-Up.

which were filled with epoxy. This bonding approach was intended to insure the maximum accuracy. In the evaporator region, the thermocouple leads passed out from underneath the pipe through small grooves in the heater blocks. Initially, some problems occurred with the thermocouples reading high along the heater block interface. This was found to be caused by poor contact at the heater block/heat pipe interface, causing the heater block to become significantly hotter (100° C) than the heat pipe. The poor contact was due to interference between the heater block and some tack welds on the heat pipe (See Figure 4-4). When these weld beads were removed, the thermocouples began to read normally. A second set of thermocouples was attached along the side of the heat pipe next to one of the liquid channels. This set of thermocouples acted as a backup for the primary thermocouples.

All the thermocouple leads fed into a floating reference junction which in turn fed the voltage differences into a data acquisition system. This data system consists of a Hewlet-Packard scanner (Model 3495A) which connects the thermocouple channels with a Hewlett-Packard Digital Voltmeter (Model 3455A). A Tektronix computer (Model 4051) was used to read the thermocouple voltage and convert them to temperature readings. The thermocouple data could then be printed onto a CRT screen or a Tektronix printer (Model 4642) by user command.

5. HEAT PIPE TESTS

The primary objective of this program was to test the channel wick heat pipe and use the test data for analyzing and developing future design approaches. Consequently, a test program was developed to investigate and analyze several design issues. Among the key issues were:

1. Do lower groove densities enhance transport as theory suggests?
2. Is transport directly proportional to channel wick evaporator heat flux as theory suggests?
3. Is boiling a major factor in transport failure?
4. Will covering grooves with a glass fiber wick enhance the liquid distribution over the groove surface and increase the pipe transport?

To evaluate the design issues, a test program was developed which analyzed the effects of groove density, evaporator heat flux, boiling, and the use of a glass fiber wick. Table 5-1 presents the program test matrix which summarizes the basic tests. The first four tests evaluated the effect of groove density and heat flux on the transport. During all tests, observations were also made to detect the presence of boiling. The last two tests evaluated the effectiveness of using a glass fiber wick underneath the cover blocks (See Figure 2-3).

In this section, the general testing approach is first discussed. This is followed by a discussion of the test results. At the end of this section the results are analyzed and compared with the theoretical models.

GENERAL TESTING APPROACHES

The primary data required for this program was the maximum heat pipe transport data. To acquire this data the following two test methods were used: (1) the power-method, and (2) the tilt-method.

In the tilt-method approach, the evaporator heater power is set and the pipe temperatures are allowed to stabilize. The pipe is then tilted about

Table 5-1 High Capacity Heat Pipe Test Plan Matrix

Test Sequence No.	Desired Results	Test Variable	
		Groove Density (Groove/cm)	Heat Flux Area (cm^2)*
1	Pipe Transport Groove Transport Groove Boiling	39	.39
2	Pipe Transport Groove Transport Groove Boiling	20	39
3	Pipe Transport Groove Transport Groove Boiling	39	77
4	Pipe Transport Groove Transport Groove Boiling	20	77
5	Pipe Transport Groove Transport Groove Boiling With Glass Fiber Wick	39	77
6	Pipe Transport Groove Transport Groove Boiling With Glass Fiber Wick	20	77

* Based on Internal Groove Exposure Area

.08 cm(.031 inch) and the temperatures allowed to adjust. About every 15 minutes, the pipe is tilted another .08 cm(.031 inch) until burnout occurs. At burnout, the ΔT across the pipe increases significantly.

There are two disadvantages to using the tilt method; the first is that the heat pipe motion can affect the determination of the burnout point. The second disadvantage is that accuracy is limited for pipes with low static heights.

In the power-method, the pipe tilt is set and a small amount of power is applied to the evaporator. When the pipe temperatures have stabilized, the power is increased. This process is repeated until burnout occurs. The primary disadvantage of this method is that burnout is not easily determined at low tilts. This is due to the good axial heat conduction and gravity flow (no capillary pumping) that masks the evaporator temperature rise of burnout.

Consequently, both of these methods were used during the program to develop and check test results.

TEST RESULTS

The first two transport test series were performed with the pipe uncanted (See Figure 4-4) and charged with 69 gm of ammonia (110% of ideal charge). In addition, only the outer heater block was used for heat input and burnout was determined by the power-method.

Figure 5-1 shows the ΔT data for the evaporator with 20 grooves/cm (50 groove in.). As can be seen, burnout was not always well defined. For example, the .32 cm (.12 in.) tilt showed burnout between 200 W and 220 W for one case and 250 W and 300 W for the other case. Also, for zero tilt, burnout appears to occur between 300 W and 350 W in one case and 350 W and 400 W in the other.

In a third test at zero tilt, the ΔT decreased between 380 W and 450 W. This was followed by an increase to 24° C at 500 W. At this point the ΔT fell to about 8° C and then increased back to 13° C. This type of be-

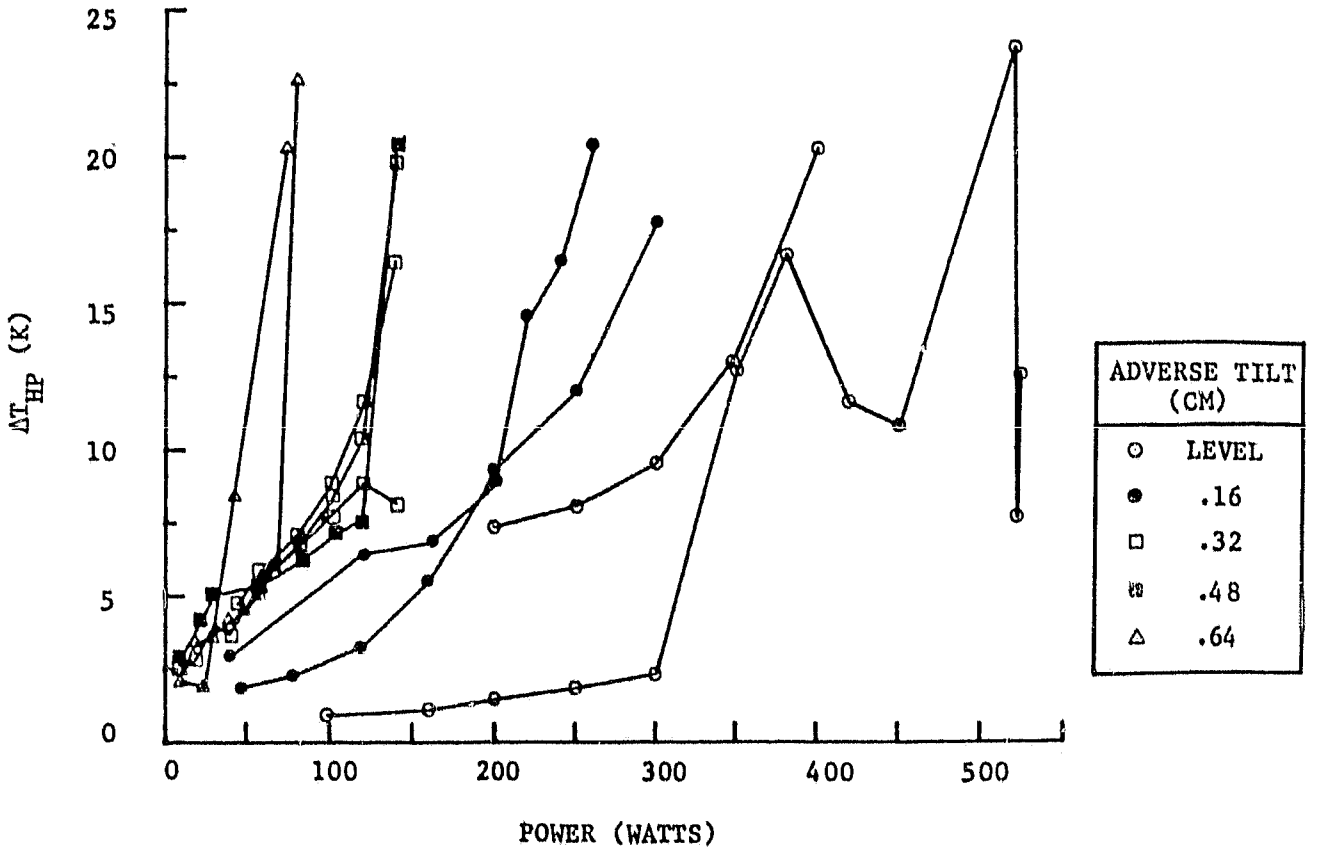

Figure 5-1 . Data for the 30 cm, 20 Groove/cm Evaporator

havior was believed to be caused by the growth and collapse of bubbles in the liquid channels. Consequently, the pipe was considered to be burned-out at the point where the ΔT initially broke away from previous trends. In addition, this test also indicates that the pipe is probably burned-out when the ΔT exceeds 8-10^{o} C.

Figure 5-2 shows similar results for the evaporator with 39 grooves/cm (100 grooves/in.). Again the zero tilt case shows burnout between 60 and 80 W in one case and 150 and 200 W in another case. The .32 and .64 cm (.12 and .25 in.) tilt tests show similar variations.

Figure 5-3 summarizes the results of these tests by plotting the pipe transport as a function of tilt. As can be seen, the 20 groove/cm (50 groove/in.) evaporator appears to perform better than the 39 groove/cm (100 groove/in.) evaporator. This observation is consistent with the predicted trends of the groove transport theory. In addition, a significant amount of boiling underneath the cover blocks was observed and this is believed to account for the variation of results.

Figure 5-3 also shows that the apparent static height of the pipe was below .79 cm (.31 in.) for both groove densities. The predicted static height for the 20 groove/cm (50 groove/in.) and 39 groove/cm (100 groove/in.) evaporators were 1.24 and 2.50 cm (.49 and .98 in.) respectively. This static height performance was probably due to flaws in the grooved surfaces which the cover blocks could not correct. This conclusion is supported by the apparent increases in pipe static height when the glass fiber wick was installed underneath the cover blocks. This improvement in static height will be discussed later in this section.

Even at these low static heights, the transport is still significantly lower than the predicted channel wick transport. For example, if a .31 cm (.12 in.) static height is assumed, then the predicted level transport is about 1400 W. Because of this erratic performance and the observations of boiling under the cover blocks, the test set-up was modified by cant-

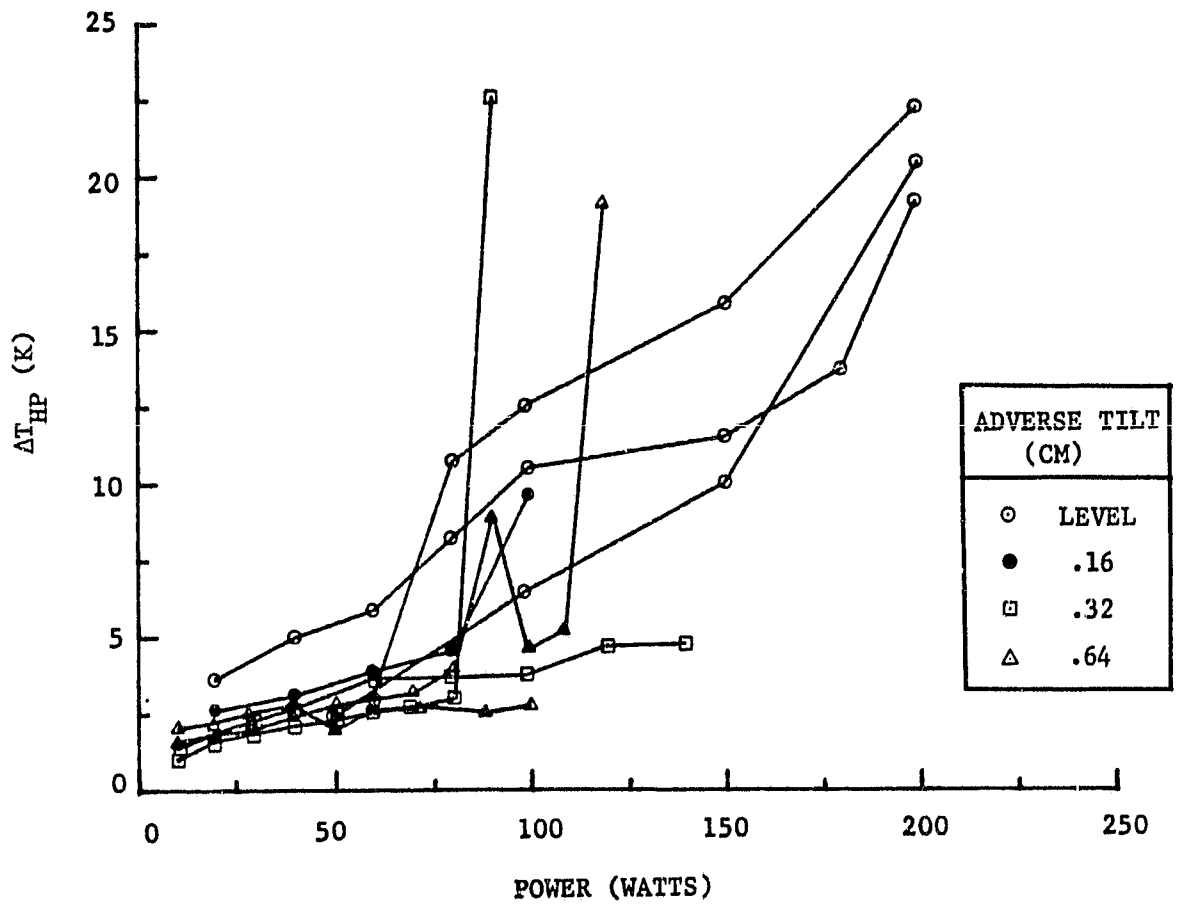

Figure 5-2. Data for the 30 cm, 39 Groove/cm Evaporator

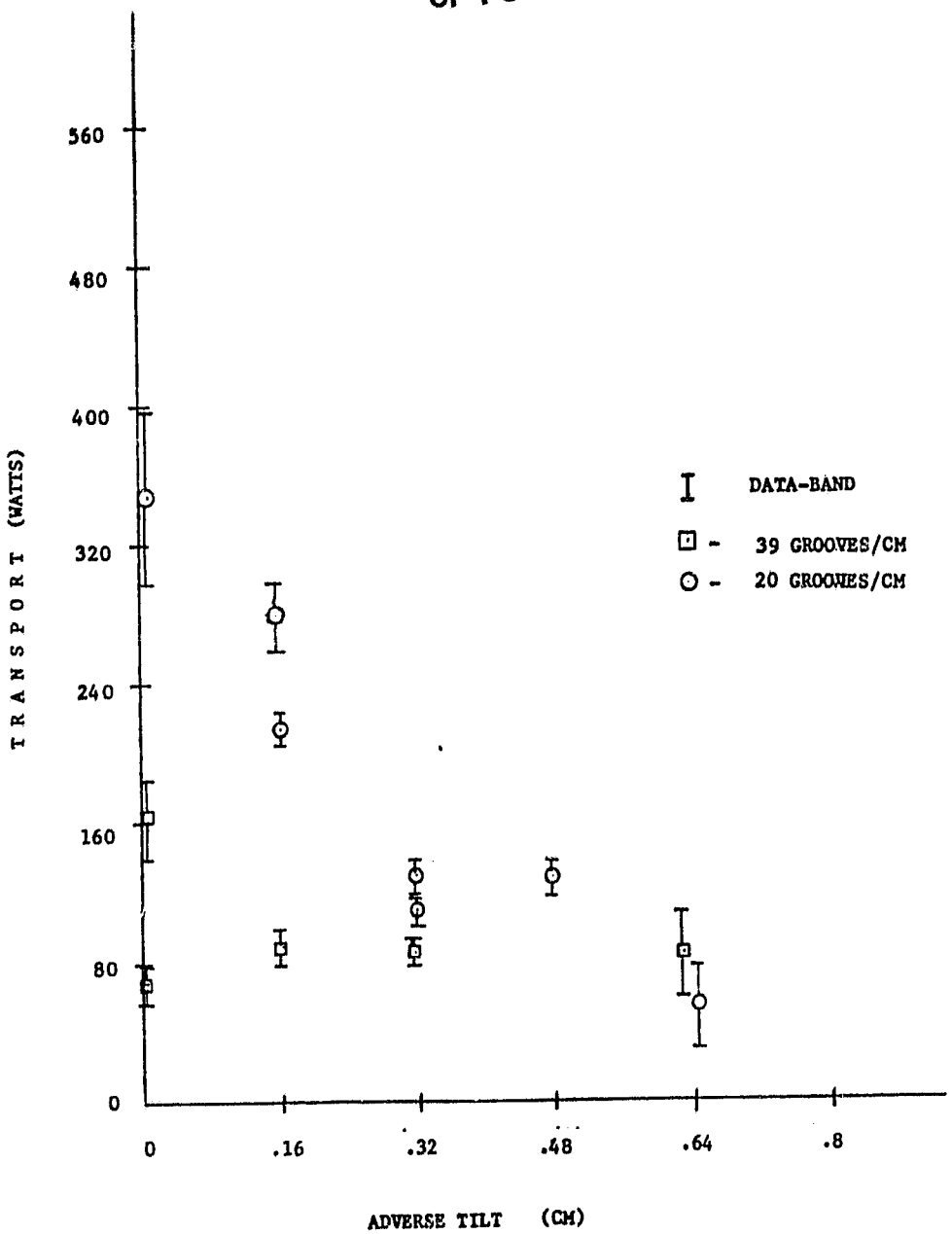

Figure 5-3 . Transport Data for the 30 cm Evaporator

ing the pipe and moving the heater block directly underneath the upper channel (See Figure 4-5). To reduce the transport of the upper channel the charge was reduced to 53 grams (84% of ideal charge). These two changes helped to reduce the possibility of boiling. Finally, the testing approach was changed to the tilt-method for determining burnout. Figure 5-4 shows the results for the 30 cm, 39 groove/cm (12 in., 50 groove/in.) evaporator. As can be seen, the pipe ΔT remains nearly constant until burnout occurs.

Figure 5-5 shows similar results for the 30 cm, 20 groove/cm (12 in., 50 groove/in.) evaporator. Since this latter test showed that the static height was about .24 cm (.094 in.), the test was repeated using the power method. These results are shown in Figure 5-6.

Again, the power method showed some variations in the results. For zero tilt, the pipe burned-out between 120 and 140 W in one case and 240 and 260 W in the second case. Note that these transport levels are lower than those for the original tests. This was expected since the canted grooves had to pump against gravity.

Figure 5-7 summarizes the transport data from these three tests. As can be seen there is some ambiguity in the results. The tests using the tilt method show that the 20 groove/cm (50 groove/in.) evaporator has a higher zero-tilt transport than the 39 groove/cm (100 groove/in.) evaporator. One of the power-method tests also showed this result. However, the remaining power method tests show that the reverse is true.

Two possible explanations for these results have been identified. First, boiling is the probable mechanism for triggering burnout; therefore, burnout could be dependent upon the conditions existing at a nucleation site or the location of a nucleation site. Consequently, burnout could occur over a range of transport values. The second possibility is that the different testing methods affected the results. This explanation would be more plausible if the power-method had generally exceeded the tilt-method test data. However, this explanation must be considered since the data generally shows

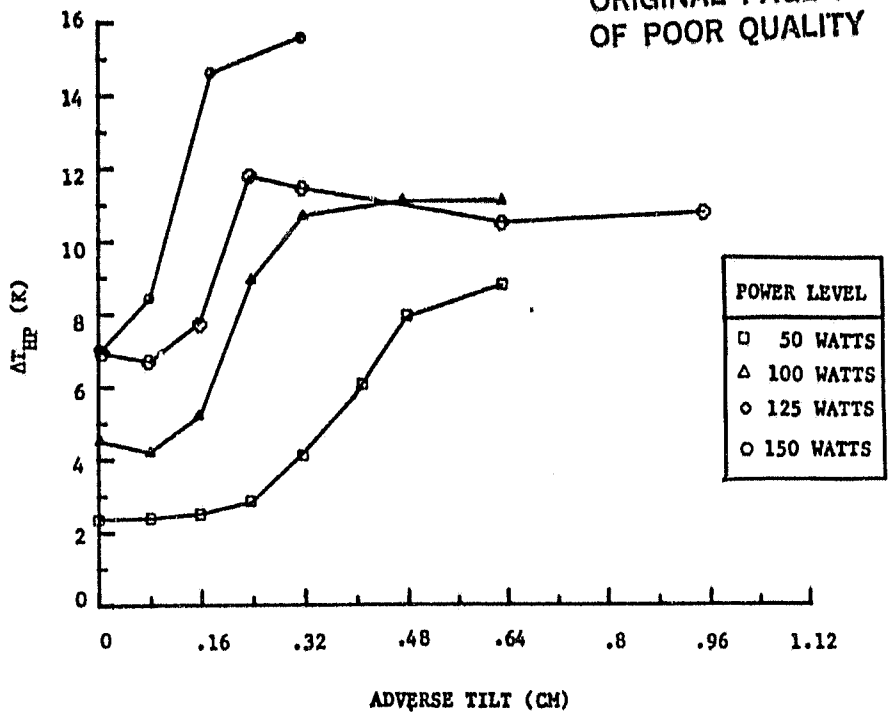

Figure 5-4 . Data for the 30 cm, 39 Groove/cm Evaporator

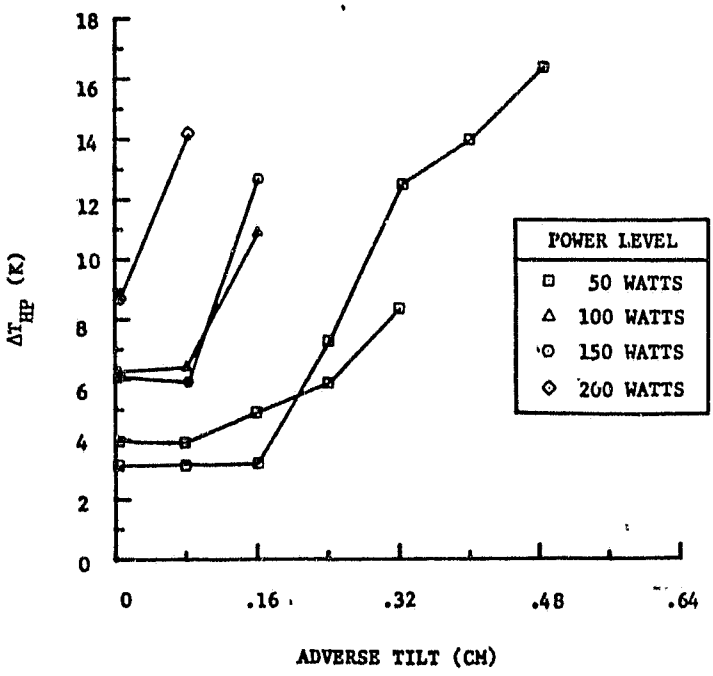

Figure 5-5 . Data for the 30 cm, 20 Groove/cm Evaporator

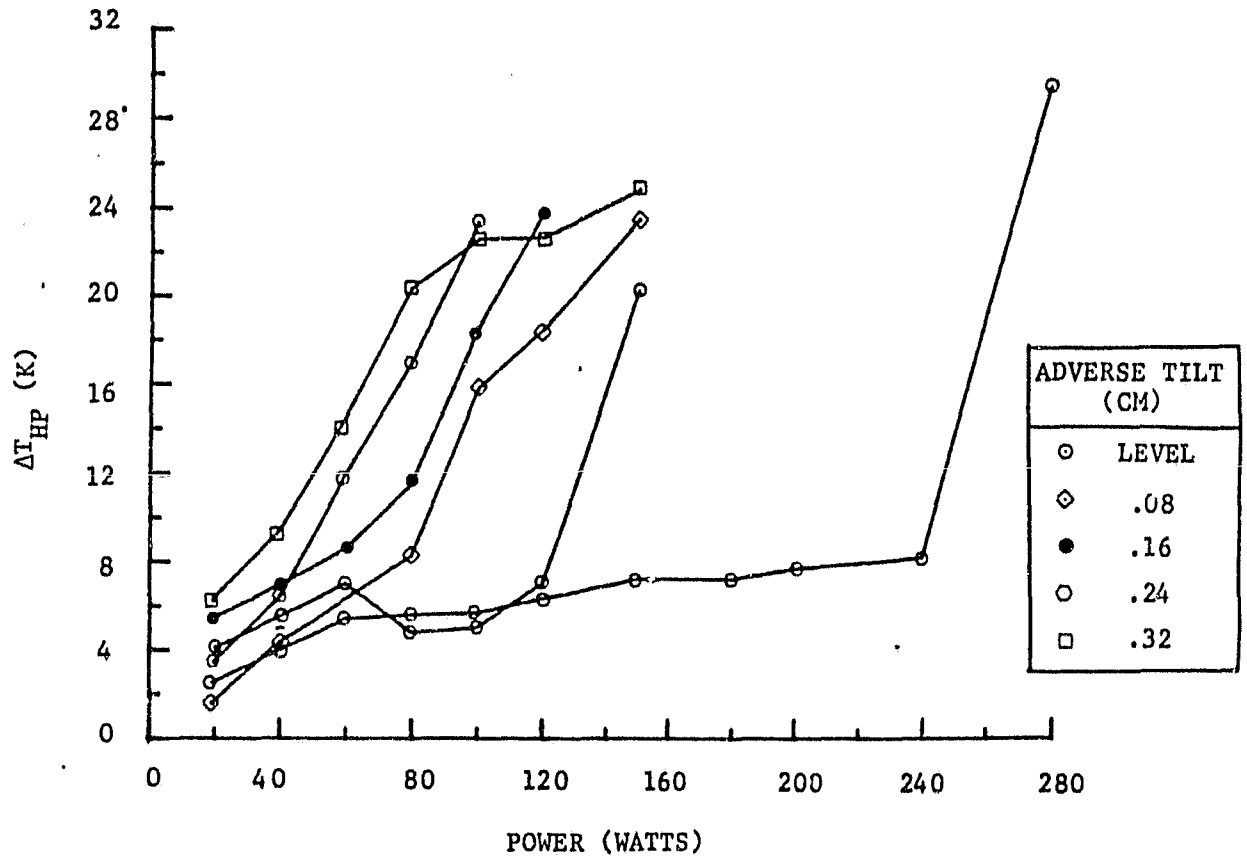

Figure 5-6 . Data for the 30 cm, 20 Groove/cm Evaporator

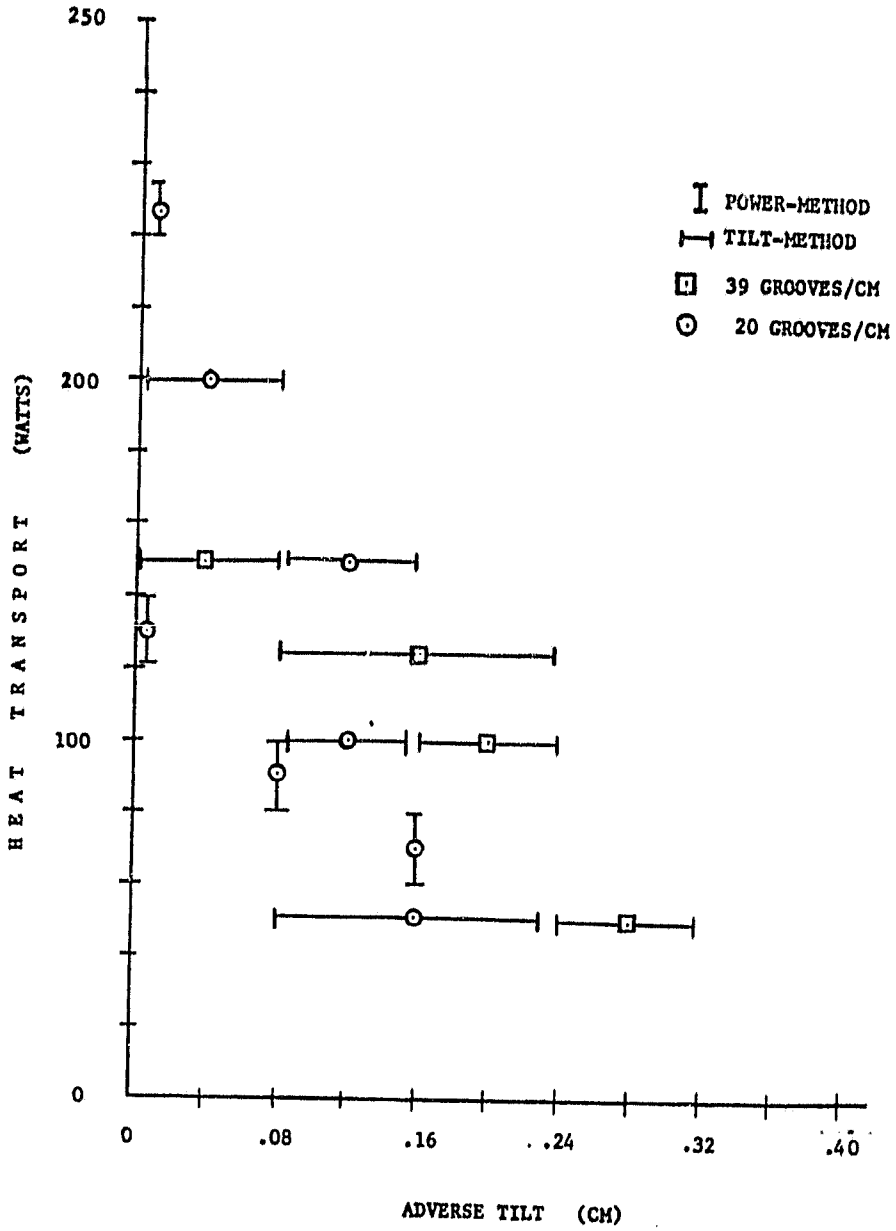

Figure 5-7. Transport Data for the 30 cm Evaporator

significant differences between the test methods.

Similar results were obtained for 61 cm (24 in.) evaporator as shown in Figures 5-8, 5-9, and 5-10. These tests also used the canted test set-up (Figure 4-5). The results of these tests are summarized in Figure 5-11, which shows the transport as a function of tilt. Again, the results are somewhat ambiguous. As can be seen, the data gathered by the tilt-method shows that the 39 groove/cm (100 groove/in.) evaporator transports slightly more than the 20 groove/cm (50 groove/in.) evaporator. However, the power method shows that in some cases the transport is about the same.

The data in Figure 5-7 and 5-11 were replotted to show how the evaporator length affected the transport. For the 39 groove/cm (100 groove/in.) evaporator, Figure 5-12 shows that the 61 cm (24 in.) evaporator had a higher transport than the 30 cm (12 in.) evaporator.

On the other hand, Figure 5-13 presents the data for the 20 groove/cm (50 groove/in.) evaporator. In one case, the transport appears to be about the same for both the 61 cm (24 in.) and 30 cm (12 in.) evaporators. In another case, the 61 cm evaporator appears to transport about half that of the 30 cm (12 in.) evaporator. This later result was in direct contradiction with the groove transport and boiling models and is discussed further in the following section.

Boiling was observed in the pipe during all these tests. For the most part, it appeared to be originating from underneath the cover blocks and purging through the grooves. Continuous boiling was observed at power levels as low as 40 W, indicating that ammonia is extremely sensitive to boiling.

The exact point at which boiling becomes destructive could not be identified. However, it appears that boiling is the probable mechanism that caused the erratic performance of the pipe.

Observations of boiling after burnout would sometime show the grooves drying out and then repriming periodically. This appeared to be due to bubble growth and collapse inside the liquid channel.

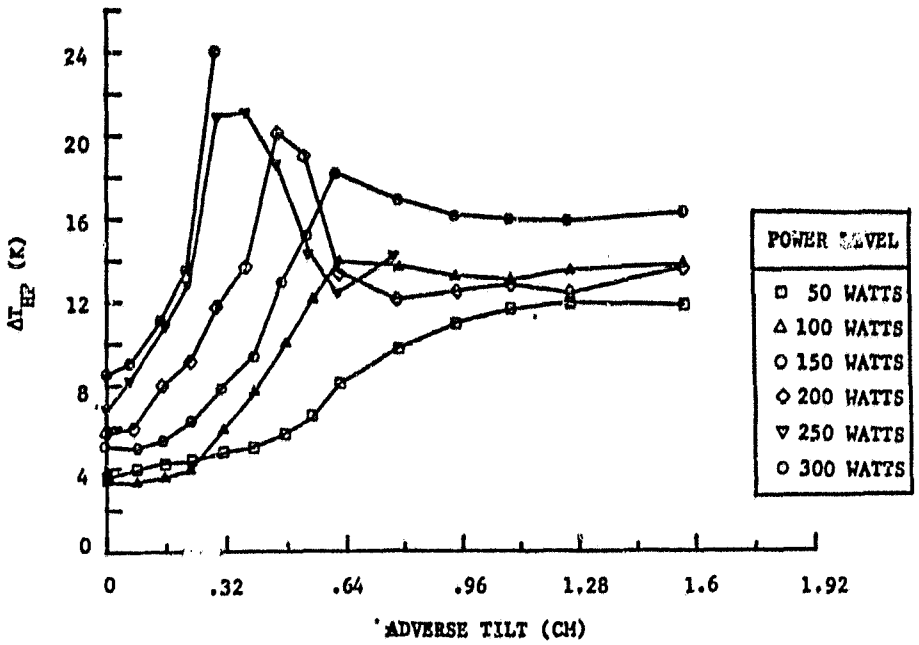

Figure 5-8. Data for the 61 cm, 39 Groove/cm Evaporator

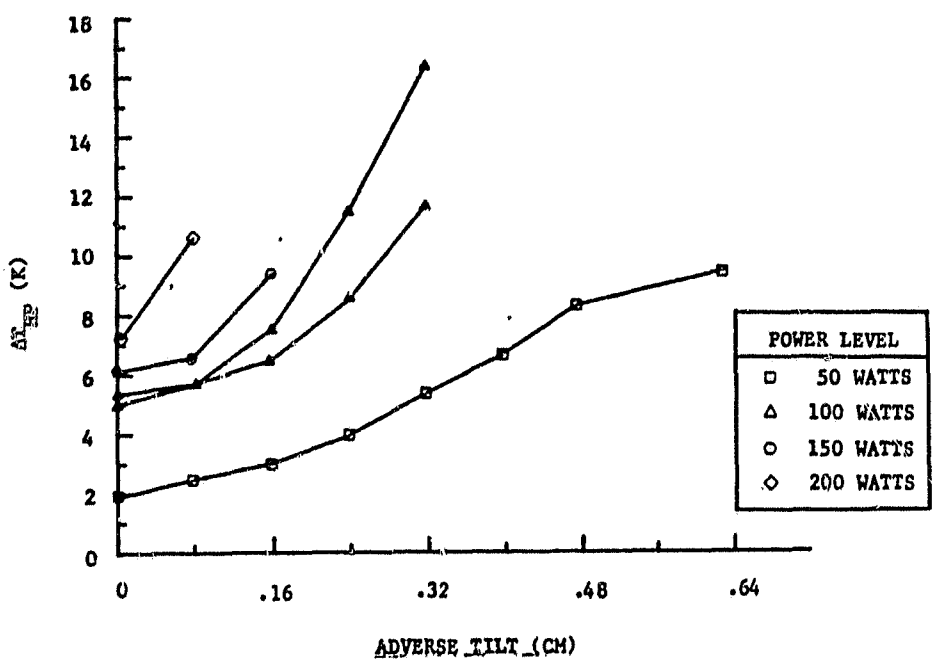

Figure 5-9. Data for the 61 cm, 20 Groove/cm Evaporator

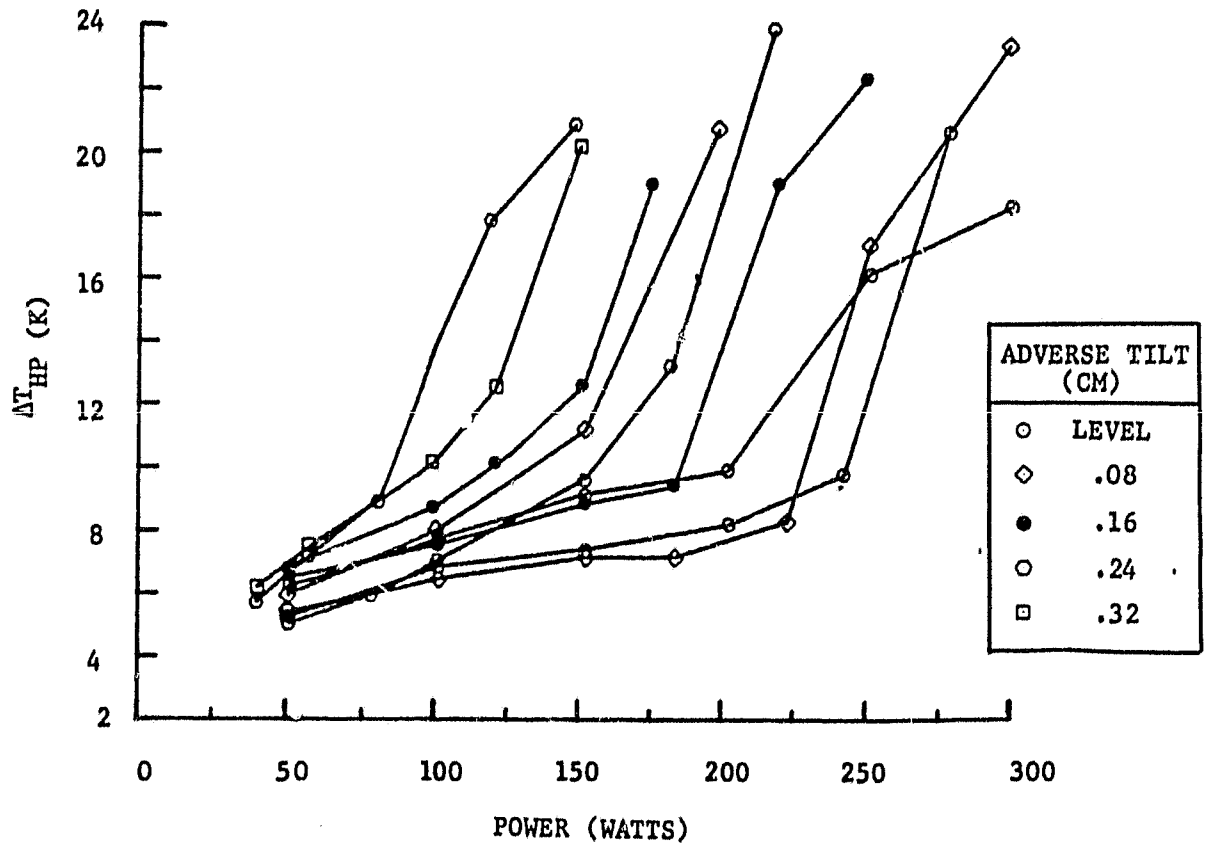

Figure 5-10.Data for the 61 cm, 20 Groove/cm Evaporator

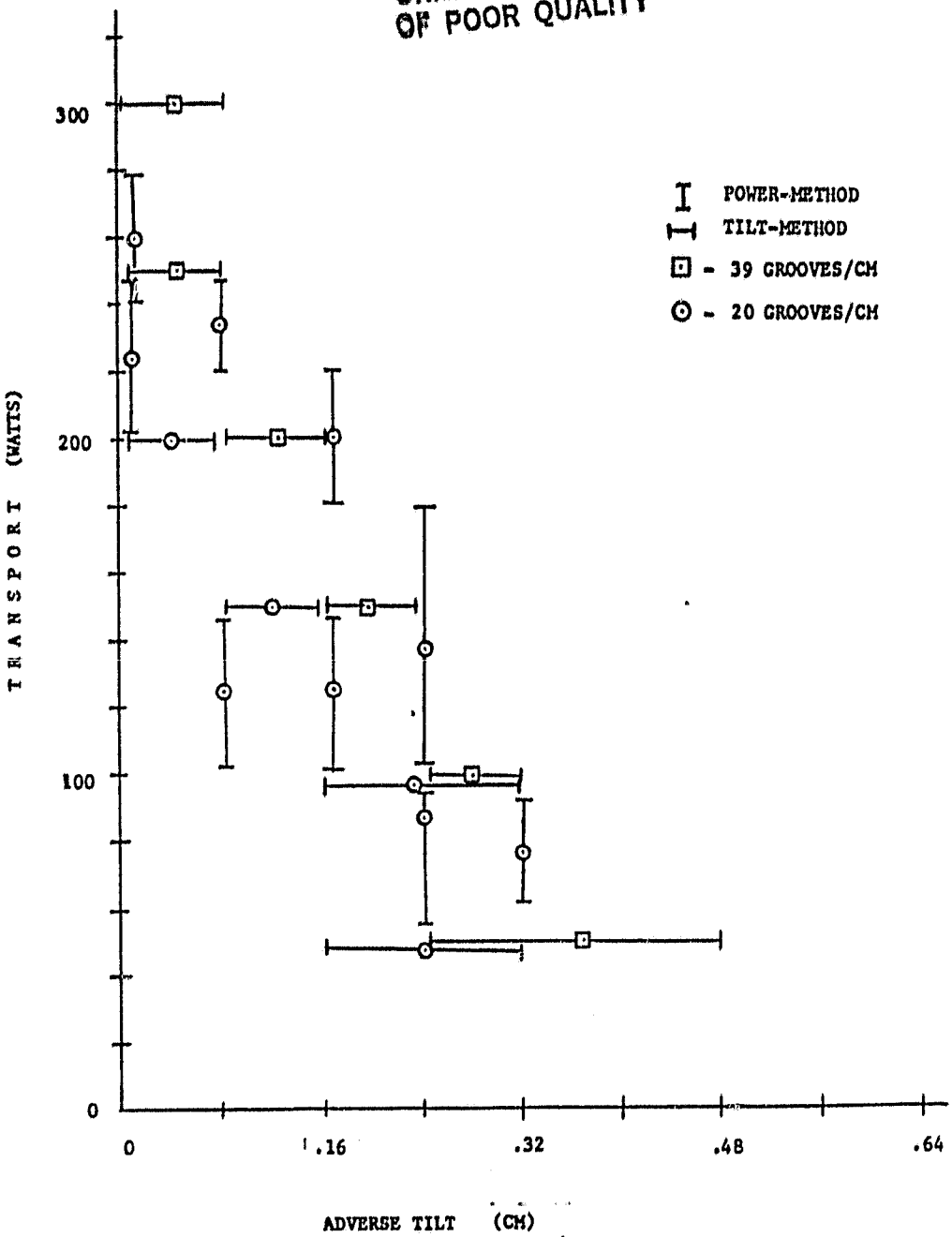

Figure 5-11. Transport Data for the 61 cm Evaporator

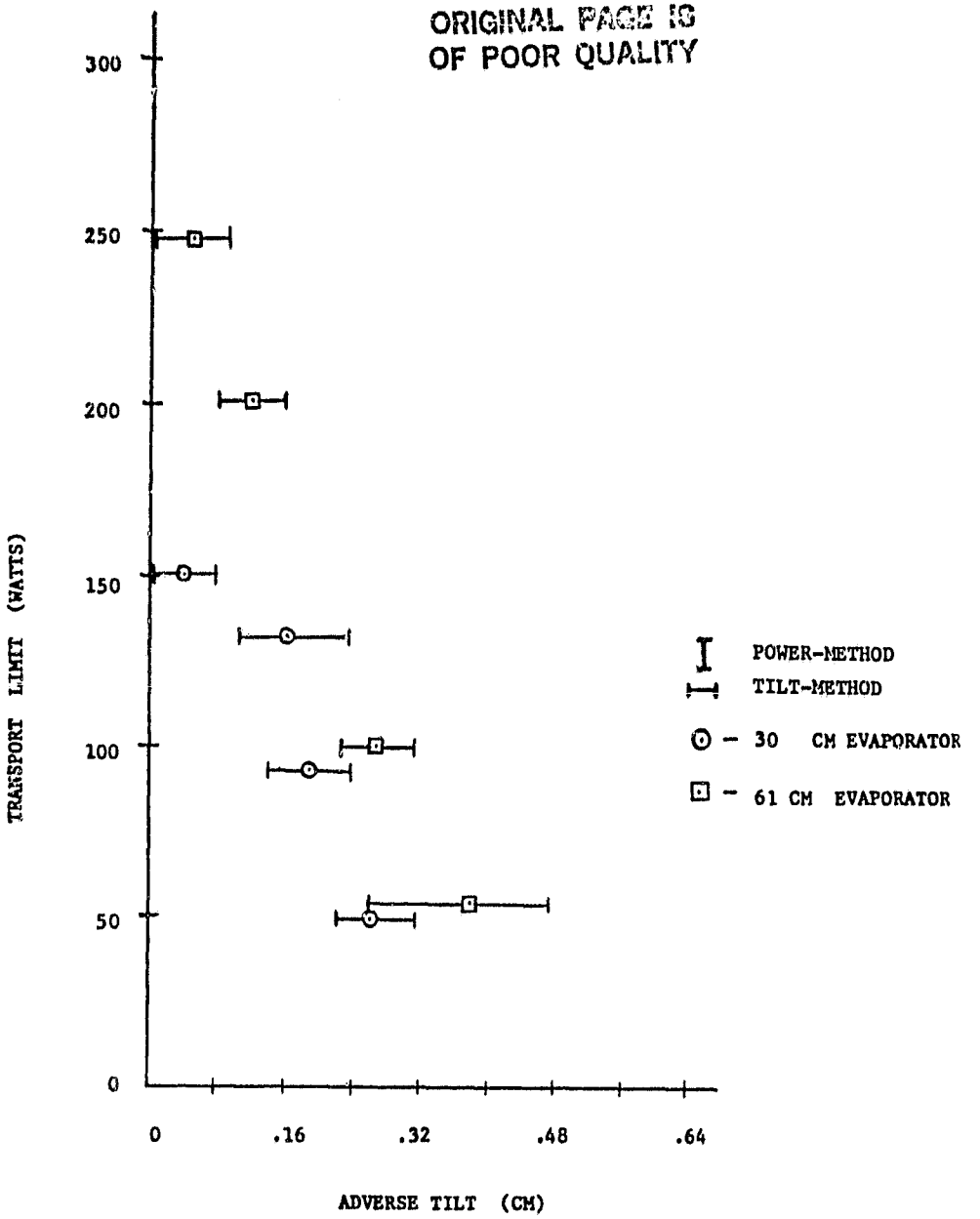

Figure 5-12. Transport Data for the 39 Groove/cm Evaporator

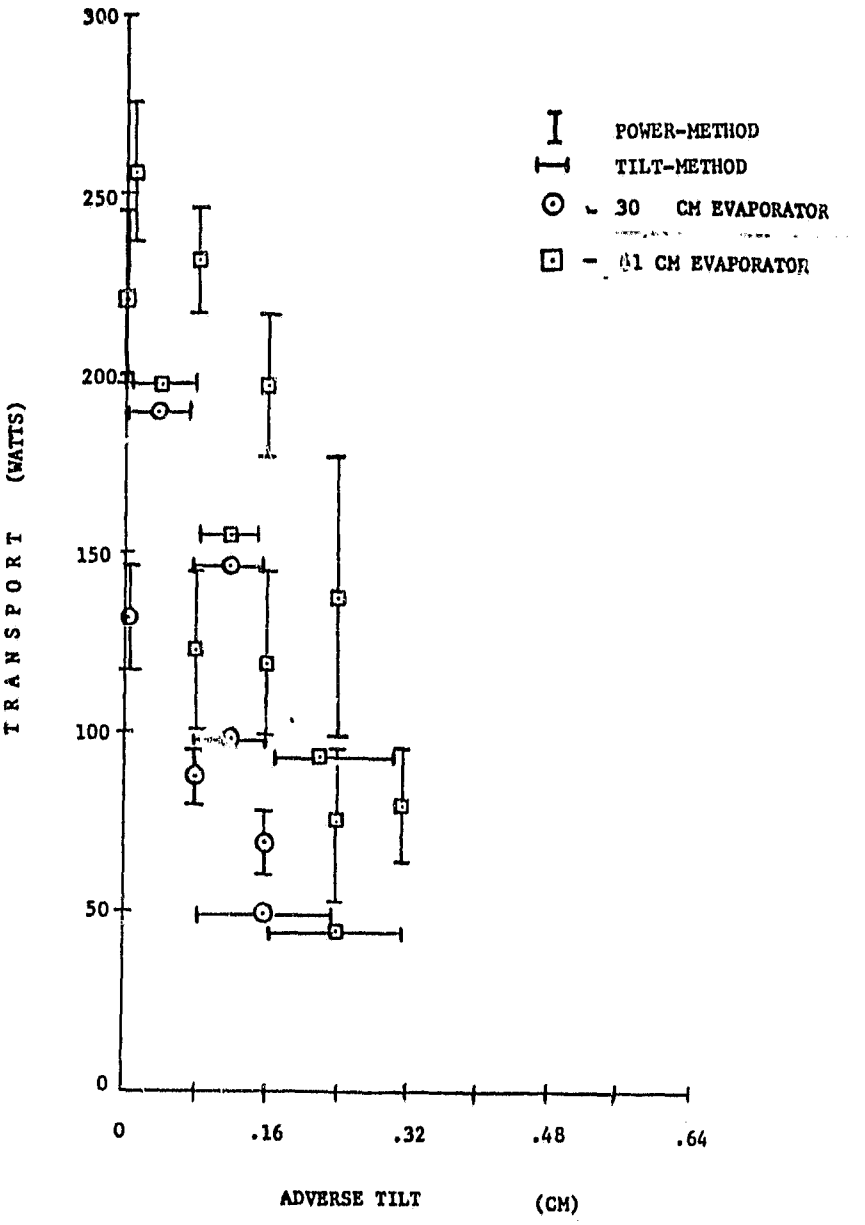

Figure 5-13. Transport Data for the 20 Groove/cm Evaporator

In addition, after the first series of tests (uncanted pipe), the ammonia was analyzed for gas contamination. This analysis showed that the ammonia had less than 5 ppm for any of the common gases (He, H_2, Ne, O_2, Ar, N_2, etc.). Consequently, neither boiling nor the performance of the pipe was due to excessive amounts of non-condensible gas.

The final two test series were performed with the glass fiber wick installed underneath the cover blocks. The pipe was tested in the uncanted position and the heater blocks centered on the evaporator slab (See Figure 4-4). Since the fill for this pipe could not be calculated accurately, the pipe was filled while observing the wetting of the evaporator grooves. This insured that the pipe had sufficient liquid in it for testing.

Figures 5-14 and 5-15 show the test data for the 20 groove/cm and 39 groove/cm (50 groove/in. and 100 groove/in.) evaporators, respectively. Both of these tests used a 61 cm (24 in.) long evaporator. As can be seen, the maximum transport is between about 120 to 140 W for both cases. In these tests the pipe appeared to perform more consistently than in previous tests. However, the overall transport was reduced from that observed for the pipe without the glass wick.

Figure 5-16 summarizes this data as a function of tilt. Note that the static heights appear significantly higher than in the previous tests. They also appear to be higher than the theoretical prediction. This last factor tends to indicate that the glass fiber wick allowed the development of an inverted meniscus. In addition, the glass penetration into the groove reduces the pore radius developed.

Finally, two additional test series were run to assess the performance with a 30 cm (12 in.) evaporator. As Figures 5-17 and 5-18 show, the performance drops off slightly (20-40 W) for the 30 cm (12 in.) evaporators. Again, the maximum transport appears to be about the same for both the 20 and 39 groove/cm (50 and 100 groove/in.) evaporators.

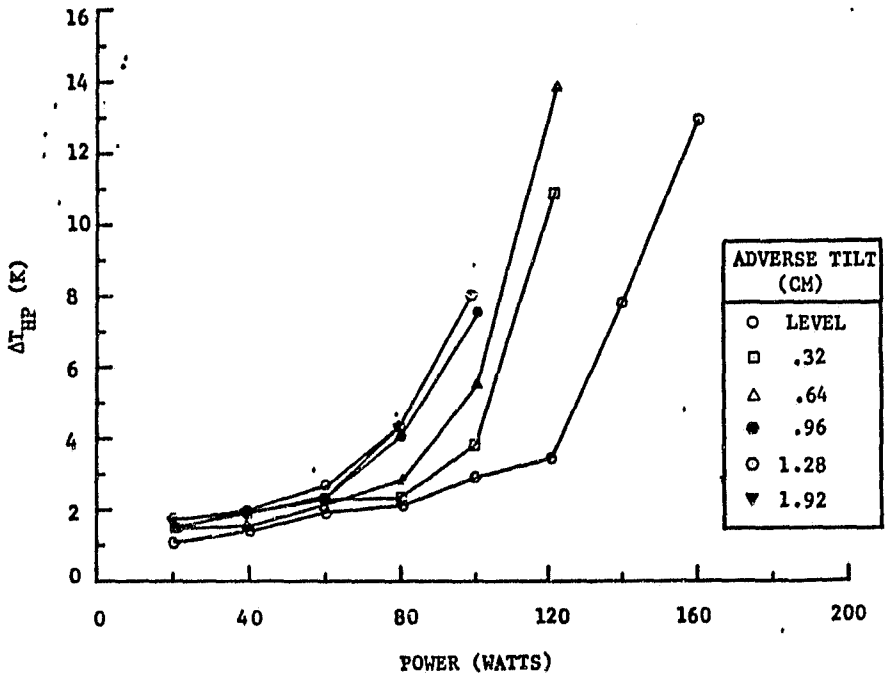

Figure 5-14. Data for the 61 cm, 20 Groove/cm Evaporator (Glass Fiber Wick)

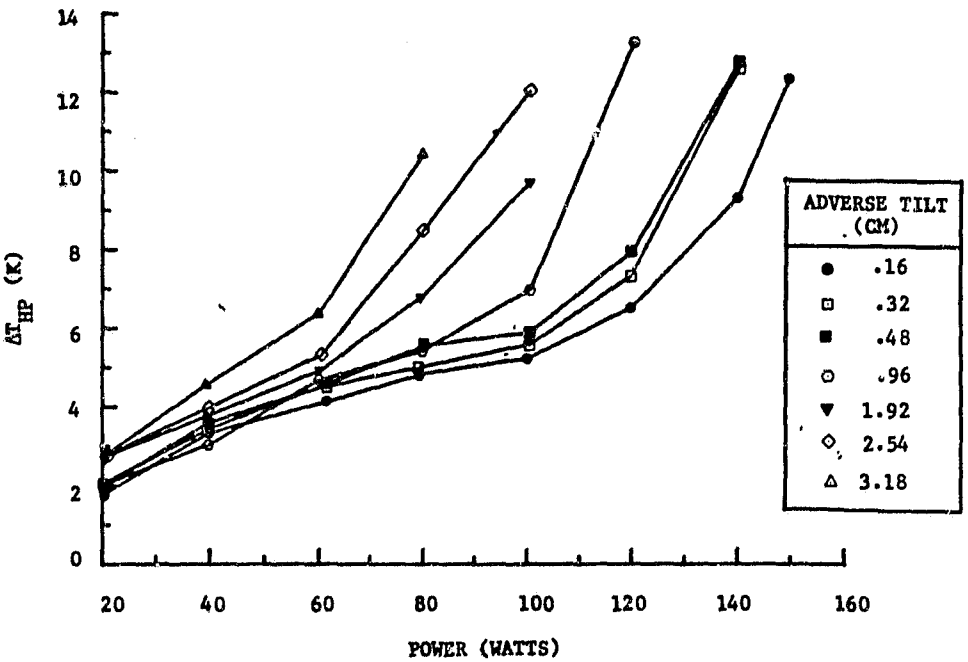

Figure 5-15. Data for the 61 cm, 39 Groove/cm Evaporator (Glass Fiber Wick)

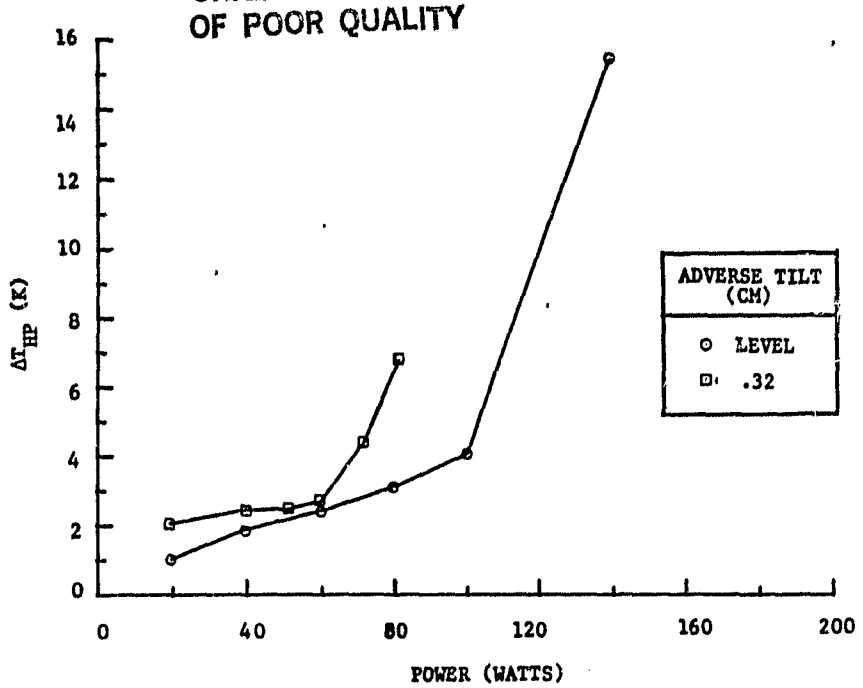

Figure 5-17. Data for the 30 cm, 20 Groove/cm Evaporator (Glass Fiber Wick)

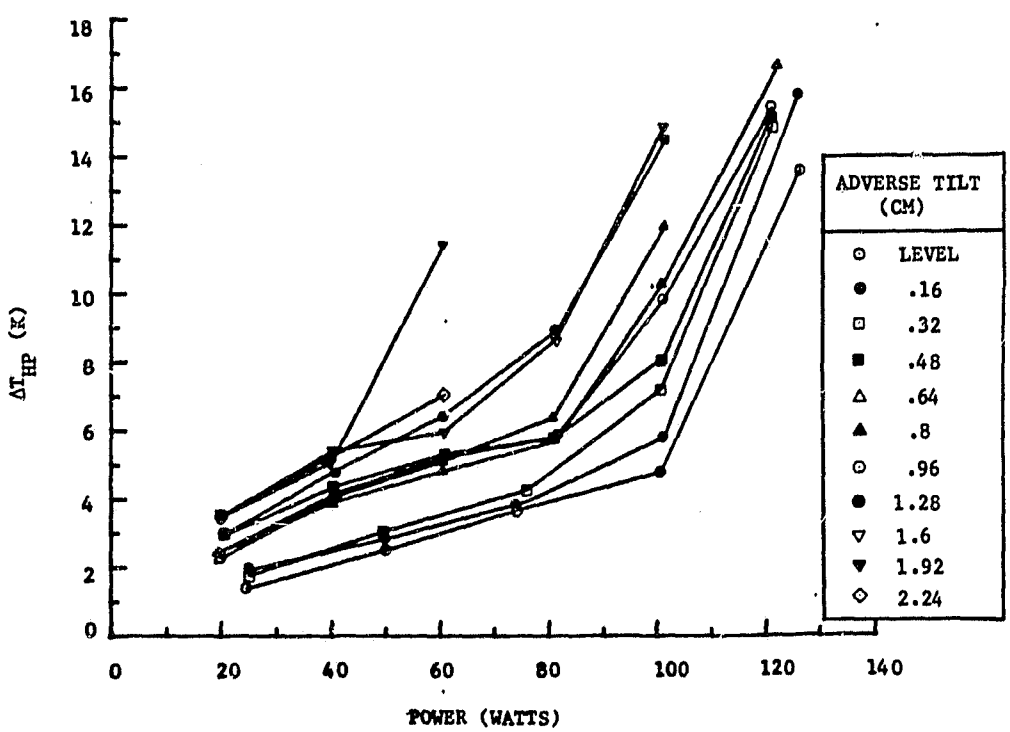

Figure 5-18. Data for the 30 cm, 39 Groove/cm Evaporator (Glass Fiber Wick)

No boiling was observed in these tests with the glass fiber wick. This could be due to the development of an inverted meniscus or to obscuration of some groove surfaces by the glass fiber wick or window fogging (See Appendix).

DISCUSSION OF RESULTS

Table 5-2 summarizes the transport results as a function of evaporator length and groove density. For tests where more than one transport value was obtained, column "a" gives the lower transport value and column "b" the higher value.

In analyzing the data in Table 5-2, several observations can be made. First, cases 1-b (row-column) and 2-a show that the transport of the 20 groove/cm (50 groove/in.) evaporator exceeded that of the 39 groove/cm (100 groove/in.) evaporator. This result is consistent with the trends predicted by the groove transport calculations.

On the other hand, cases 1-a, and 2-a in Table 5-2 show that the 39 groove/cm (100 groove/in.) evaporator slightly exceeded the 20 groove/cm (50 groove/in.) evaporator. This type of behavior is more consistent with the boiling model. However, it can be seen that the transport is not proportional to the groove density as the model predicts.

The most plausible explanation for relating cases 1-a, 1-b, and 2-a is that boiling is not a single valued function as depicted by the simplified boiling model. Instead, boiling is probably a much more complicated process involving considerations such as nucleation pore conditions, nucleation point location, local temperature gradients and history, and trace amounts of non-condensible gas. Consequently, transport failure could occur over a range of power levels. In the cases where boiling did not induce transport failure early, then the groove transport characteristics would allow the performance to be enhanced. This explanation would account for the transport characteristics exhibited in case 1-b.

Table 5-2 Summary of Transport Results

Row	Evaporator Length (inches)	Groove Density (grooves/cm)	Transport (watts)	
			a	b
1	30	20	100-140 W	200-220 W
2	30	39	150-170 W	
3	61	20	100-150 W*	240-280 W
4	61	39	250-280 W	

* May be due to poor recovery from prior test.

Cases 3-b and 4-a in Table 5-2 show essentially the same transport. As shown in Section 3, poorer quality grooves show less sensitivity to groove density. However, cases 1-b and 2-a do not support this conclusion. Therefore, a more likely hypothesis is that a maximum superheat condition exists such that groove failure is induced. In examining Figures 5-8, 5-9, and 5-10, failure appears to occur when the pipe ΔT is about 7^{o} C. Therefore, boiling appears to be the most plausible failure mechanism. Again, this data tends to discount the groove model where the boiling limit is directly proportional to the groove density.

On the other hand, cases 3-a and 4-a show boiling to be directly proportional to groove density; but cases 3-a and 1-b directly contradict the proportional relationship of evaporator length. Two possibilities exist for explaining this data. First, this could be further evidence that boiling is not a single valued limit, thus supporting the previous data. Second, in Figure 5-11, only one data point tends to support the 100-150 W transport value. This point is the .08 cm (.031 in.) tilt data point. Examining the curve related to this data point in Figure 5-10 shows that the initial slope is higher than most of the other curves in the figure. Consequently, there is a possibility that this point did not fully recover from the previous test.

If boiling is the cause of burnout, then the next question is, "what causes the variations in performance?" Potentially, there are several factors which could affect performance. First, the design of the modified channel wick heat pipe might contribute to these performance variations. In particular, the cover blocks could pose problems in venting vapor bubbles. As illustrated in Figure 5-19, a vapor bubble could expand back into the liquid channel prior to venting. If this occured, then capillary pumping would be destroyed and burnout would occur. This process would depend on the nucleation sight location and its conditions. In addition, transport would depend on which nucleation site would dominate in a particular test.

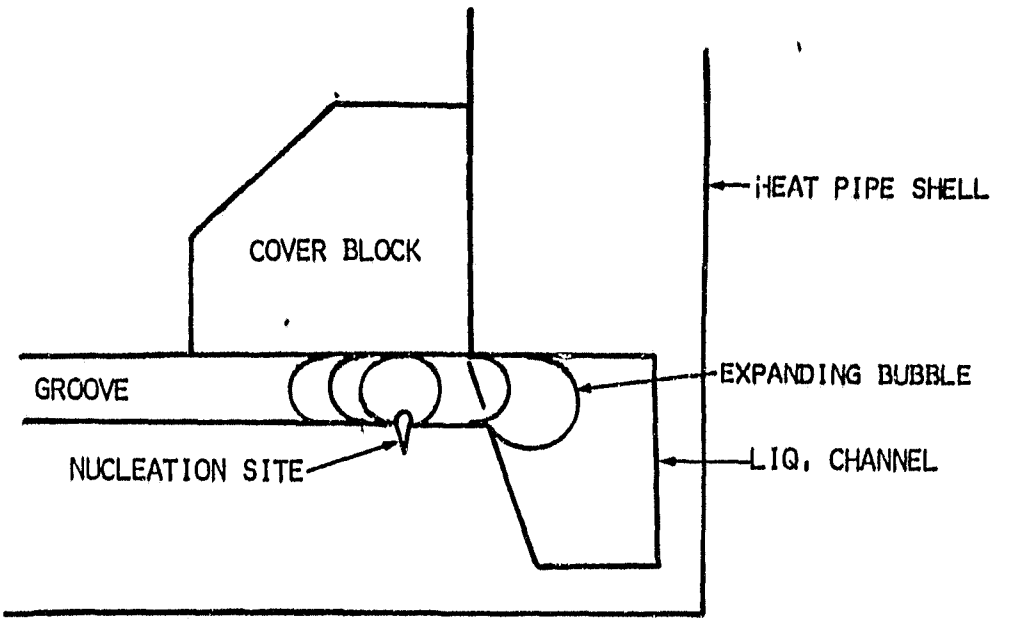

Figure 5-19. Bubble Induced Transport Failure.

In addition to the heat pipe design, several other factors could affect the transport. These include the nucleation site wall temperature, liquid temperature, and trace amounts of gas which either evolves from the liquid or at the nucleation sites. This last factor may be an important factor with respect to bubble formation at the nucleation sites. Edward Kroliczek of the OAO Corporation believes that non-condensible gas can evolve in an ammonia heat pipe at concentration levels as low as 50-1000 ppm. This belief is based on some of the work done by Saaski (Reference 3). However, further work is required to fully assess this problem.

For the last two test series, no definite signs of boiling were observed. However, from the previous tests, it seems highly probable that boiling did occur. Also, a more restrictive venting path would be expected due to the glass fiber penetration into the groove. Therefore, this could explain the lower transport performance.

Future Design Considerations

Based on the results of these tests, several design suggestions can be made for future high capacity heat pipes using v-groove surfaces. First, the liquid channels should be well isolated from the heating interface. Figure 5-20 shows an example of this for the channel wick concept. In this design, the isolation slots have been widened to reduce the heat flow into the channels and maximize the vaporization efficiency.

Next, the groove cover blocks should be eliminated. This minimizes the possibility of a vapor bubble being blown back into the channel and causing the pipe to deprime.

A glass fiber wick is an excellent concept for generating an inverted meniscus. However, its use should be limited to concepts which do not allow the possibility of a bubble being blown back into the main pumping channel or artery. This minimizes the problems due to boiling and non-condensible gas.

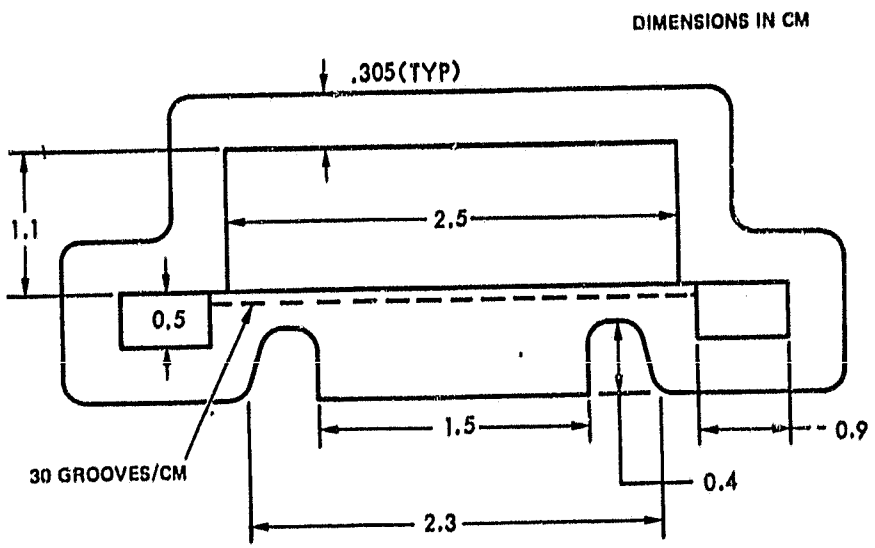

Figure 5-20. Improved Channel Wick Design

From Table 5-2, it can be seen that the 20 groove/cm (50 groove/in.) evaporator was more prone to performance variations than the 39 groove/cm (100 groove/in.) evaporator. On the other hand, there was evidence that the 20 groove/cm (50 groove/in.) evaporator could be desirable. It is believed that boiling was the primary factor limiting performance in this program. Consequently, if the above suggestions did eliminate the problems with boiling, then a 20 groove/cm (50 groove/in.) evaporator could improve the overall pipe performance. However, initial design approaches should probably use a 30 groove/cm (75 groove/in.) evaporator to minimize risk.

Finally, consideration should be given to the potential gas problem. This problem is still not fully understood and the design approaches need to be further defined.

6. CONCLUSIONS

Basically, this test program showed that boiling is probably the key factor limiting evaporator transport. This was supported by observation of continuous boiling at power levels as low as 40 W and test data which appears to vary over a range of power levels. These variations tend to indicate that boiling may depend upon several factors including pipe design and nucleation site conditions. Therefore, from a practical standpoint, the simple boiling model based on wall superheat has limited application in heat pipe design.

There was also indication that lower groove densities will enhance the groove transport if boiling can be minimized or eliminated. This was shown in the tests with a 30 cm evaporator. Here the transport increased from 150-170 W to 200-220 W when the groove density went from 39 groove/cm (100 groove/in.) to 20 groove/cm (50 groove/in.). However, due to transport variation, this result was not a consistent trend throughout the test program, lending further support for boiling as the primary failure mechanism.

Similarly, there was some support for the transport being proportional to evaporator length. As shown for the 39 groove/cm (100 groove/in.) evaporator, the transport increased from 150-170 W to 250-280 W as the evaporator length was increased from 30 cm (12 in.) to 61 cm (24 in.).

For the pipe with the glass fiber wick installed, a relatively low transport was obtained. For the 61 cm (24 in.) evaporator, a transport of 120-140 W was obtained for both groove densities. Similarly, the 30 cm (12 in.) evaporator showed a transport of 100-120 W for both groove densities.

Based on these results and the identification of some potential causes for them, several future design suggestions were developed. These included (1) better thermal isolation of the liquid channels, (2) elimination of the groove cover blocks,(3) elimination of the glass fiber wick

from channel-wick type designs, and (4) the use of lowest groove density which is not limited by boiling.

7. RECOMMENDATIONS

Several key questions still remain in respect to grooved heat pipe evaporators and boiling. Among them are:

- o Would other fluids improve the performance?
- o Do the cover blocks definitely affect performance?
- o When does boiling become destructive?
- o What effect does gas have on boiling?
- o What causes the transport variations?
- o What effect does groove surface quality have on boiling?

To address these questions and to further understand the results, the following recommendations are made:

1. Groove transport tests should be made with other heat pipe fluids such as acetone.
2. The pipe should be re-tested without the cover blocks to assess the boiling problem.
3. Models of gas bubble growth and collapse need to be developed to assess the effect of gas on boiling.
4. Additional groove transport tests need to be performed to assess the causes of the transport variations and how the surface quality effects transport. These tests should be performed in a specially designed test fixture which allows various test samples to be tested.

REFERENCES

1. Bahr, A., E. Burck, W. Hufschmidt, Liquid-Vapor Interaction and Evaporation In Heat Pipes, presented at the 2nd International Conference on Thermionic Electric Power Generation, Paper No. D-6, May 27-31, 1968.
2. Lehtinen, A.M., Passive Thermal Control Systems Technology - Final IR&D Report for CFY 1981, January 1982.
3. Saaski, E.W., Investigation of Bubbles in Arterial Heat Pipes, NASA CR 114,531, 1972.

APPENDIX

POLYSULFONE WINDOW DEGRADATION

Initially, polysulfone was identified as a compatible window material for exposure to saturated ammonia. However, during the tests the optical quality of the window began to slowly degrade. This degradation appeared as a light-colored opaque area which began and spread throughout the evaporator section. The area most affected by this degradation was the hot end of the evaporator. During burnout, temperatures in this area were allowed to rise 10-30° C above the ambient temperature. This tends to indicate that the degradation process is a sensitive function of temperature.

When the windows on the pipe were replaced, this degradation was determined to be caused by fine micro-cracks on the interior of the window. Fine cracks on the window surface are believed to be the initiation points for this interior cracking. In addition, local swelling of the polysulfone windows appeared in the areas exposed to the ammonia. Whether this swelling was due to the cracking or a cause of the cracking was not determined.

Figure A-1 shows a typical degraded window along with a cross section of the degraded area.

ORIGINAL PAGE
BLACK AND WHITE PHOTOGRAPH

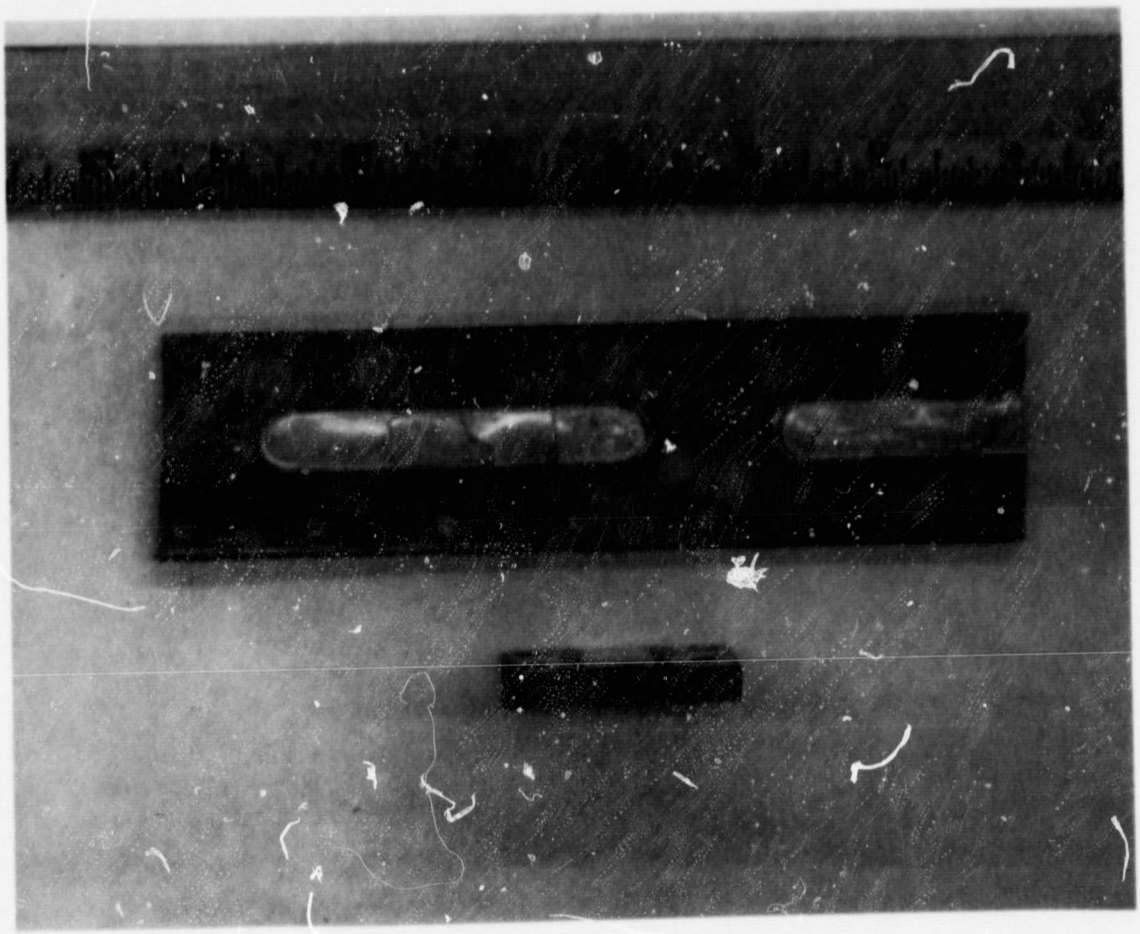

Figure A-1. Polysulfone Window Degradation